Beyond the relativistic mean-field approximation. III. Collective Hamiltonian in five dimensions

Nikšić, Tamara; Li, Z. P.; Vretenar, Dario; Prochniak, L.; Meng, Jie; Ring, Peter

Beyond the relativistic mean-field approximation. III. Collective Hamiltonian in five dimensions

T. Nikšić, Z. P. Li,[*] and D. Vretenar

Physics Department, Faculty of Science, University of Zagreb, Croatia

L. Próchniak

Institute of Physics, Maria Curie-Sklodowska University, Lublin, Poland

J. Meng

School of Physics, Peking University, Beijing, People's Republic of China

P. Ring

Physik-Department der Technischen Universität München, Garching, Germany

The framework of relativistic energy density functionals is extended to include correlations related to the restoration of broken symmetries and fluctuations of collective variables. A new implementation is developed for the solution of the eigenvalue problem of a five-dimensional collective Hamiltonian for quadrupole vibrational and rotational degrees of freedom, with parameters determined by constrained self-consistent relativistic mean-field calculations for triaxial shapes. The model is tested in a series of illustrative calculations of potential energy surfaces and the resulting collective excitation spectra and transition probabilities of the chain of even-even gadolinium isotopes.

I. INTRODUCTION

Nuclear structure models based on energy density functionals (EDFs) have successfully been used over the whole nuclide chart, from relatively light systems to superheavy nuclei, and from the valley of β stability to the particle drip lines [1–3]. In lowest order, i.e., the mean-field approximation, an EDF is constructed as a functional of one-body nucleon density matrices that correspond to a single product state—the Slater determinant of single-particle or single-quasiparticle states. This framework can thus also be referred to as a single-reference (SR) EDF. The static nuclear mean field is characterized by symmetry breaking—translational, rotational, and particle number. Even though symmetry breaking incorporates important static correlations, i.e., deformations and pairing in the SR EDF, this framework can only describe ground-state properties such as binding energies and charge radii. Excitation spectra and electromagnetic transition probabilities can only be calculated by including correlations beyond the static mean field through the restoration of broken symmetries and configuration mixing of symmetry-breaking product states. The most effective approach to configuration mixing calculations is the generator coordinate method (GCM) [4], with multipole moments used as collective coordinates that generate the symmetry-breaking product wave functions. In such a multireference (MR) EDF approach, families of static mean-field configurations are mixed to restore symmetries and to take into account fluctuations of collective variables.

The corresponding EDFs are functionals of transition densities built from pairs of symmetry-breaking product states.

In the first two parts of this work [5,6], we extended the framework of relativistic energy density functionals to include correlations related to the restoration of broken symmetries and to fluctuations of collective variables. A model has been developed that uses the GCM to perform configuration mixing of angular-momentum and particle-number projected relativistic wave functions. The geometry is restricted to axially symmetric shapes, and the intrinsic wave functions are generated from the solutions of the relativistic mean-field+Lipkin-Nogami BCS equations, with a constraint on the mass quadrupole moment. The model employs a relativistic point-coupling (contact) nucleon-nucleon effective interaction in the particle-hole channel, and a density-independent δ interaction in the particle-particle channel. This approach enables a quantitative description of the evolution of shell structure, deformation, and shape coexistence phenomena in nuclei with soft potential energy surfaces.

In the first application [7], the GCM based on relativistic EDFs was employed in a study of shape transitions in Nd isotopes. It has been shown that the microscopic framework based on universal EDFs, adjusted to nuclear ground-state properties, and extended to take into account correlations related to symmetry restoration and fluctuations of collective variables, describes not only general features of shape transitions but also the unique behavior of the excitation spectra and transition rates at the X(5) critical point of the quantum shape phase transition. However, an exact diagonalization of the X(5) Hamiltonian carried out in Ref. [8] has shown that many properties of the solution are dominated by β-γ coupling induced by the kinetic energy operator. The importance of the explicit treatment of the triaxial degree of freedom, i.e.,

---

*Current address: School of Physics, Peking University, Beijing, China.

inclusion of β-γ coupling, was also emphasized in two recent studies of shape transitions in the Nd isotopic chain [9, 10], which used the self-consistent Hartree-Fock-Bogoliubov model, based on the finite-range and density-dependent Gogny interaction, to generate potential energy surfaces in the β-γ plane.

While GCM configuration mixing of axially symmetric mean-field states has been implemented by several groups and routinely used in nuclear structure studies, the application of this method to triaxial shapes is a much more difficult problem. Only very recently a model has been introduced [11] based on the mean-field states generated by triaxial quadrupole constraints that are projected on particle number and angular momentum and mixed by the generator coordinate method. This method is equivalent to a seven-dimensional GCM calculation, mixing all five degrees of freedom of the quadrupole operator and the gauge angles for protons and neutrons. However, the numerical implementation of the model is very complex, and applications to medium-heavy and heavy nuclei are still computationally too demanding and time consuming. In addition, the use of general EDFs, i.e., with an arbitrary dependence on nucleon densities, in GCM-type calculations often leads to discontinuities or even divergences of the energy kernels as a function of deformation [12,13]. Only for certain types of density dependence can a regularization method be implemented [14], which corrects energy kernels and removes the discontinuities and divergences.

In an alternative approach to five-dimensional quadrupole dynamics that includes rotational symmetry restoration and takes into account triaxial quadrupole fluctuations, a collective Bohr Hamiltonian is constructed, with deformation-dependent parameters determined from microscopic self-consistent mean-field calculations [15,16]. The collective Hamiltonian can be derived in the Gaussian overlap approximation (GOA) [4] to the full five-dimensional GCM. With the assumption that the GCM overlap kernels can be approximated by Gaussian functions, the local expansion of the kernels up to second order in the nonlocality transforms the GCM Hill-Wheeler equation into a second-order differential equation—the Schrödinger equation for the collective Hamiltonian. The kinetic part of this Hamiltonian contains an inertia tensor [17], and the potential energy is determined by the diagonal elements of the Hamiltonian kernel, and the collective energy surface also includes zero-point energy (ZPE) corrections [18]. The adiabatic time-dependent Hartree-Fock (ATDHF) theory [19] provides an alternative way to derive a classical collective Hamiltonian, and, after requantization, a Bohr Hamiltonian of the same structure is obtained but with different microscopic expressions for the inertia parameters [20]. There is a long-standing debate in the literature about masses in the collective Bohr Hamiltonian [21], i.e., whether the GCM-GOA expressions (the so-called Yoccoz masses [22]) or the ATDHF expressions (the so-called Thouless-Valatin masses [23]) should be used. The Thouless-Valatin masses have the advantage that they also include the time-odd components of the microscopic wave functions and, in this sense, the full dynamics of a nuclear system. In the GCM approach, these components can only be included if, in addition to the coordinates q_i, the corresponding canonically

conjugate momenta p_i are also taken into account, but this is obviously a very complicated task. In many applications a further simplification is thus introduced in terms of cranking formulas [18,24], i.e., the perturbative limit for the Thouless-Valatin masses, and the corresponding expressions for ZPE corrections. This approximation was applied in recent studies using models based on both the Gogny interaction [25] and Skyrme energy density functionals [26].

In this work, we develop a new implementation for the solution of a five-dimensional collective Hamiltonian that describes quadrupole vibrational and rotational degrees of freedom, with parameters determined in the framework of relativistic EDF. An initial study along this line, which, however, did not include ZPE corrections, was reported in Ref. [27].

The theoretical framework is described in Sec. II: the method of solution of the eigenvalue problem of the general collective Hamiltonian, and the calculation of the mass parameters, moments of inertia, and ZPE corrections. In Sec. III the model is tested in the calculation of collective excitation spectra of the chain of even-even Gd isotopes, and results are compared with available data. Section IV presents a summary and an outlook for future studies. Technical details about the solution of the Dirac equation in triaxial geometry, the calculation of moments of inertia, ZPE corrections, and numerical tests are included in Appendix A–D.

II. THEORETICAL FRAMEWORK

A. Collective Hamiltonian in five dimensions

Nuclear excitations determined by quadrupole vibrational and rotational degrees of freedom can be treated simultaneously by considering five quadrupole collective coordinates $\alpha_\mu, \mu = -2, -1, \ldots, 2$, that describe the surface of a deformed nucleus: $R = R_0[1 + \sum_\mu \alpha_\mu Y^*_{2\mu}]$. To separate rotational and vibrational motion, these coordinates are usually parametrized in terms of two deformation parameters β and γ and three Euler angles $(\phi, \theta, \psi) \equiv \Omega$, which define the orientation of the intrinsic principal axes in the laboratory frame,

$$\alpha_\mu = D^2_{\mu 0}(\Omega)\beta \cos\gamma + \frac{1}{\sqrt{2}}\big[D^2_{\mu 2}(\Omega) + D^2_{\mu -2}(\Omega)\big]\beta \sin\gamma, \tag{1}$$

where $D^\lambda_{\mu\nu}$ is the Wigner function [28]. The three terms of the classical collective Hamiltonian, expressed in terms of the intrinsic variables β, γ and Euler angles as

$$H_{\text{coll}} = \mathcal{T}_{\text{vib}}(\beta, \gamma) + \mathcal{T}_{\text{rot}}(\beta, \gamma, \Omega) + \mathcal{V}_{\text{coll}}(\beta, \gamma), \tag{2}$$

denote the contributions from the vibrational kinetic energy

$$\mathcal{T}_{\text{vib}} = \tfrac{1}{2} B_{\beta\beta}\dot\beta^2 + \beta B_{\beta\gamma}\dot\beta\dot\gamma + \tfrac{1}{2}\beta^2 B_{\gamma\gamma}\dot\gamma^2, \tag{3}$$

the rotational kinetic energy

$$\mathcal{T}_{\text{rot}} = \frac{1}{2}\sum_{k=1}^{3}\mathcal{I}_k\omega_k^2, \tag{4}$$

and the collective potential energy $\mathcal{V}_{\text{coll}}(\beta, \gamma)$. The mass parameters $B_{\beta\beta}, B_{\beta\gamma}, B_{\gamma\gamma}$, and the moments of inertia $\mathcal{I}_k$ depend on the quadrupole deformation variables β and γ.

The Hamiltonian (2) is quantized according to the general Pauli prescription [29]: for the classical kinetic energy,

$$T = \frac{1}{2}\sum_{ij} B_{ij}(q)\dot{q}_i\dot{q}_j, \quad (5)$$

and the corresponding quantized form reads

$$\hat{H}_{\text{kin}} = -\frac{\hbar^2}{2}\frac{1}{\sqrt{\det B}}\sum_{ij}\frac{\partial}{\partial q_i}\sqrt{\det B}(B^{-1})_{ij}\frac{\partial}{\partial q_j}. \quad (6)$$

The kinetic energy tensor in Eq. (2) takes the block diagonal form

$$B = \begin{pmatrix} B_{\text{vib}} & 0 \\ 0 & B_{\text{rot}} \end{pmatrix}, \quad (7)$$

with the vibrational part of the tensor

$$B_{\text{vib}} = \begin{pmatrix} B_{\beta\beta} & \beta B_{\beta\gamma} \\ \beta B_{\beta\gamma} & \beta^2 B_{\gamma\gamma} \end{pmatrix}. \quad (8)$$

In general, the rotational part is a complicated function of the Euler angles, but, using the quasicoordinates related to the components of the angular momentum in the body-fixed frame, it takes a simple diagonal form

$$(B_{\text{rot}})_{ik} = \delta_{ik}\mathcal{I}_k, \quad k = 1, 2, 3, \quad (9)$$

with the moments of inertia expressed as

$$\mathcal{I}_k = 4B_k\beta^2\sin^2(\gamma - 2k\pi/3). \quad (10)$$

This particular functional form is motivated by the fact that all three moments of inertia vanish for the spherical configuration ($\beta = 0$), and, additionally, $\mathcal{I}_z$ and $\mathcal{I}_y$ vanish for axially symmetric prolate ($\gamma = 0°$) and oblate ($\gamma = 60°$) configurations, respectively. The resulting determinant reads

$$\det B = \det B_{\text{vib}} \times \det B_{\text{rot}} = 4wr\beta^8\sin^2 3\gamma, \quad (11)$$

where $w = B_{\beta\beta}B_{\gamma\gamma} - B_{\beta\gamma}^2$ and $r = B_1 B_2 B_3$. The quantized collective Hamiltonian can hence be written in the form

$$\hat{H} = \hat{T}_{\text{vib}} + \hat{T}_{\text{rot}} + V_{\text{coll}}, \quad (12)$$

with

$$\hat{T}_{\text{vib}} = -\frac{\hbar^2}{2\sqrt{wr}}\left\{ \frac{1}{\beta^4}\left[\frac{\partial}{\partial\beta}\sqrt{\frac{r}{w}}\beta^4 B_{\gamma\gamma}\frac{\partial}{\partial\beta} \right.\right.$$

$$\left. - \frac{\partial}{\partial\beta}\sqrt{\frac{r}{w}}\beta^3 B_{\beta\gamma}\frac{\partial}{\partial\gamma} \right] + \frac{1}{\beta\sin 3\gamma}\left[-\frac{\partial}{\partial\gamma} \right.$$

$$\left.\left. \times \sqrt{\frac{r}{w}}\sin 3\gamma B_{\beta\gamma}\frac{\partial}{\partial\beta} + \frac{1}{\beta}\frac{\partial}{\partial\gamma}\sqrt{\frac{r}{w}}\sin 3\gamma B_{\beta\beta}\frac{\partial}{\partial\gamma} \right]\right\},$$

$$(13)$$

and

$$\hat{T}_{\text{rot}} = \frac{1}{2}\sum_{k=1}^{3}\frac{\hat{J}_k^2}{\mathcal{I}_k}, \quad (14)$$

where $\hat{J}_k$ denotes the components of the angular momentum in the body-fixed frame of a nucleus. V_{coll} is the collective potential. The Hamiltonian describes quadrupole vibrations, rotations, and the coupling of these collective modes. The determinant in Eq. (11) determines the volume element in the collective space,

$$\int d\tau_{\text{coll}} = \int d\Omega \, d\tau_0\sqrt{wr}$$

$$= \int_0^\infty d\beta \, \beta^4 \int_0^{2\pi} d\gamma |\sin 3\gamma| \int d\Omega\sqrt{wr}, \quad (15)$$

and the quantized Hamiltonian of Eq. (12) is Hermitian with respect to the collective measure in Eq. (15).

The methods used to solve the eigenvalue problem of the general collective Hamiltonian Eq. (12) can be divided into two classes. The first is based on a direct numerical solution of a system of partial differential equations using finite-difference methods [30–32]. The second approach uses an expansion of eigenfunctions in terms of a complete set of basis functions that depend on the deformation variables β and γ and the Euler angles ϕ, θ, and ψ [33–36]. The eigenvalue problem reduces to a simple matrix diagonalization, and the main task is the construction of an appropriate basis for each value of the angular-momentum quantum number.

In this work, we employ the second approach and construct basis states according to the method described in Refs. [25,36–39]. For each value of the angular momentum I, one chooses a complete set of square integrable functions

$$\phi_{Lmn}^{IM}(\beta, \gamma, \Omega) = e^{-\mu^2\beta^2/2}\beta^n \begin{Bmatrix} \cos m\gamma \\ \sin m\gamma \end{Bmatrix} D_{ML}^{I*}(\Omega). \quad (16)$$

The projections M and L are determined by the angular momentum: $M, L = -I, \ldots, I$. In principle, the parameter n can take any non-negative integer value, but in actual calculations a certain cutoff value $n_{\max}$ has to be imposed. The allowed values of m are $m = n, n - 2, \ldots, 0$ or 1. The choice of the function $e^{-\mu^2\beta^2/2}$ ensures that the basis states generate wave functions that vanish at large deformations ($\beta \to \infty$). The basis parameter μ has to be adjusted for each nucleus individually, so that it minimizes the ground-state energy of the nucleus. However, if the cutoff value $n_{\max}$ is large enough, a stable ground-state solution can be found for a broad range of values of the parameter μ.

The basis states have to fulfill certain symmetry conditions that originate from the fact that the choice of the body-fixed frame is not unique. For a given quadrupole tensor α_μ in the laboratory frame, there are 24 possible orientations of the body-fixed right-hand coordinate system, corresponding to different values of the variables β, γ, and Ω. The basis states in the body-fixed frame must be invariant with respect to the transformations that connect various choices of the body-fixed frame, and which form a finite group isomorphic to the octahedral point group O [30,40] (group of proper rotations

that takes a cube or octahedron into itself). This symmetry condition is fulfilled by linear combinations of the states (16)

$$\xi_{Lmn}^{IM}(\beta, \gamma, \Omega) = e^{-\mu^2 \beta^2 / 2} \beta^n \sum_{K \in \Delta I} f_{LmK}^I(\gamma) \Phi_{MK}^I(\Omega), \quad (17)$$

invariant under the transformations of the octahedral group. The angular part corresponds to linear combinations of the Wigner functions

$$\Phi_{MK}^I(\Omega) = \sqrt{\frac{2I+1}{16\pi^2(1+\delta_{K0})}} \left[D_{MK}^{I*}(\Omega) + (-1)^I D_{M-K}^{I*}(\Omega) \right], \quad (18)$$

and the summation in Eq. (17) is over the allowed set of the K values:

$$\Delta I = \begin{cases} 0, 2, \dots, I & \text{for } I \bmod 2 = 0, \\ 2, 4, \dots, I-1 & \text{for } I \bmod 2 = 1. \end{cases} \quad (19)$$

In the next step, linearly independent functions have to be selected from the over-complete basis set Eq. (17). In addition, some of the basis states have to be discarded to enforce the correct behavior of solutions on the $\gamma = n\pi/3$ axes [30]. A simple and elegant solution of both problems is provided by group theoretical methods [41]. Finally, the basis states of Eq. (17) are not orthogonal. Although the Hamiltonian could also be diagonalized directly in a nonorthogonal basis [35], we choose to orthogonalize the basis states by applying the Cholesky-Banachiewicz method [42].

The diagonalization of the collective Hamiltonian yields the energy spectrum E_α^I and the corresponding eigenfunctions

$$\Psi_\alpha^{IM}(\beta, \gamma, \Omega) = \sum_{K \in \Delta I} \psi_{\alpha K}^I(\beta, \gamma) \Phi_{MK}^I(\Omega). \quad (20)$$

Using the collective wave functions (20), various observables can be calculated and compared with experimental results. For instance, the quadrupole $E2$ reduced transition probability:

$$B(E2; \alpha I \to \alpha' I') = \frac{1}{2I+1} |\langle \alpha' I' \| \hat{\mathcal{M}}(E2) \| \alpha I \rangle|^2, \quad (21)$$

and the spectroscopic quadrupole moment of the state $|\alpha I\rangle$:

$$Q_{\text{spec}, \alpha I} = \frac{1}{\sqrt{2I+1}} C_{II20}^{II} \langle \alpha I \| \hat{\mathcal{M}}(E2) \| \alpha I \rangle, \quad (22)$$

where $\hat{\mathcal{M}}(E2)$ denotes the electric quadrupole operator. Detailed expressions for the reduced matrix element $\langle \alpha' I' \| \hat{\mathcal{M}}(E2) \| \alpha I \rangle$ can be found in Ref. [30].

The shape of a nucleus can be characterized in a qualitative way by average values of the invariants β^2, $\beta^3 \cos 3\gamma$, as well as their combinations. For example, the average value of the invariant β^2 in the state $|\alpha I\rangle$

$$\langle \beta^2 \rangle_{I\alpha} = \langle \Psi_\alpha^I | \beta^2 | \Psi_\alpha^I \rangle = \sum_{K \in \Delta I} \int \beta^2 |\psi_{\alpha, K}^I(\beta, \gamma)|^2 d\tau_0, \quad (23)$$

and the average values of the deformation parameters β and γ in the state $|\alpha I\rangle$ are calculated from

$$\langle \beta \rangle_{I\alpha} = \sqrt{\langle \beta^2 \rangle_{I\alpha}}, \quad (24)$$

$$\langle \gamma \rangle_{I\alpha} = \frac{1}{3} \arccos \frac{\langle \beta^3 \cos 3\gamma \rangle_{I\alpha}}{\sqrt{\langle \beta^2 \rangle_{I\alpha} \langle \beta^4 \rangle_{I\alpha}}}. \quad (25)$$

The mixing of different intrinsic configurations in the state $|\alpha I\rangle$ can be determined from the distribution of the projection K of the angular momentum I on the z axis in the body-fixed frame:

$$N_K = 6 \int_0^{\pi/3} \int_0^\infty |\psi_{\alpha, K}^I(\beta, \gamma)|^2 \beta^4 |\sin 3\gamma| d\beta \, d\gamma, \quad (26)$$

where the components $\psi_{\alpha, K}^I(\beta, \gamma)$ are defined in Eq. (20). For large deformations, the K quantum number is to a good approximation conserved. Consequently, only one of the integrals of Eq. (26) will give a value close to unity. A broader distribution of N_K values in the state $|\alpha I\rangle$ provides a measure of mixing of intrinsic configurations.

B. Parameters of the collective Hamiltonian

The entire dynamics of the collective Hamiltonian is governed by the seven functions of the intrinsic deformations β and γ: the collective potential, the three mass parameters $B_{\beta\beta}$, $B_{\beta\gamma}$, $B_{\gamma\gamma}$, and the three moments of inertia $\mathcal{I}_k$. These functions are determined by the choice of a particular microscopic nuclear energy density functional or effective interaction. As in our previous two studies of configuration mixing effects [5,6], in this work we also use the relativistic functional PC-F1 (point-coupling Lagrangian) [43] in the particle-hole channel, and a density-independent δ force is the effective interaction in the particle-particle channel. The parameters of the PC-F1 functional and the pairing strength constants V_n and V_p have been adjusted simultaneously to the nuclear matter equation of state and to ground-state observables (binding energies, charge and diffraction radii, surface thickness, and pairing gaps) of spherical nuclei [43], with pairing correlations treated in the BCS approximation.

The choice of the point-coupling effective Lagrangian determines the self-consistent relativistic mean-field (RMF) energy of a nuclear system in terms of local single-nucleon densities and currents:

$$\begin{aligned} E_{\text{RMF}} &= \int d\mathbf{r} \, \mathcal{E}_{\text{RMF}}(\mathbf{r}) \\ &= \sum_k \int d\mathbf{r} \, v_k^2 \, \bar{\psi}_k(\mathbf{r})(-i\boldsymbol{\gamma}\boldsymbol{\nabla} + m) \psi_k(\mathbf{r}) \\ &\quad + \int d\mathbf{r} \left(\frac{\alpha_S}{2} \rho_S^2 + \frac{\beta_S}{3} \rho_S^3 + \frac{\gamma_S}{4} \rho_S^4 + \frac{\delta_S}{2} \rho_S \triangle \rho_S \right. \\ &\quad + \frac{\alpha_V}{2} j_\mu j^\mu + \frac{\gamma_V}{4} (j_\mu j^\mu)^2 + \frac{\delta_V}{2} j_\mu \triangle j^\mu \\ &\quad + \frac{\alpha_{\text{TV}}}{2} j_{\text{TV}}^\mu (j_{\text{TV}})_\mu + \frac{\delta_{\text{TV}}}{2} j_{\text{TV}}^\mu \triangle (j_{\text{TV}})_\mu + \frac{\alpha_{\text{TS}}}{2} \rho_{\text{TS}}^2 \\ &\quad + \left. \frac{\delta_{\text{TS}}}{2} \rho_{\text{TS}} \triangle \rho_{\text{TS}} + \frac{e}{2} \rho_p A^0 \right), \end{aligned} \quad (27)$$

where ψ denotes the Dirac spinor field of a nucleon. The local isoscalar (S) and isovector scalar (TS) densities, and corresponding isoscalar and isovector (TV) currents for a nucleus with A nucleons

$$\rho_S(\mathbf{r}) = \sum_k v_k^2 \, \bar{\psi}_k(\mathbf{r}) \psi_k(\mathbf{r}), \quad (28)$$

$$\rho_{\text{TS}}(\boldsymbol{r}) = \sum_k v_k^2 \, \bar{\psi}_k(\boldsymbol{r}) \tau_3 \psi_k(\boldsymbol{r}), \tag{29}$$

$$j^\mu(\boldsymbol{r}) = \sum_k v_k^2 \, \bar{\psi}_k(\boldsymbol{r}) \gamma^\mu \psi_k(\boldsymbol{r}), \tag{30}$$

$$j_{\text{TV}}^\mu(\boldsymbol{r}) = \sum_k v_k^2 \, \bar{\psi}_k(\boldsymbol{r}) \gamma^\mu \tau_3 \psi_k(\boldsymbol{r}), \tag{31}$$

are calculated in the *no-sea* approximation: the summation in Eqs. (27)–(31) runs over all occupied states in the Fermi sea, i.e., only occupied single-nucleon states with positive energy explicitly contribute to the nucleon densities and currents. v_k^2 denotes the occupation factors of single-nucleon states. In Eq. (27), ρ_p is the proton density, and A^0 denotes the Coulomb potential. α, β, γ, and δ denote the 11 parameters of the PC-F1 relativistic density functional in the corresponding space-isospace channels.

The single-nucleon wave functions represent self-consistent solutions of the Dirac equation:

$$\{\boldsymbol{\alpha} \cdot [-i\boldsymbol{\nabla} - \boldsymbol{V}(\boldsymbol{r})] + V(\boldsymbol{r}) + \beta(m + S(\boldsymbol{r}))\}\psi_i(\boldsymbol{r}) = \epsilon_i \psi_i(\boldsymbol{r}). \tag{32}$$

The scalar and vector potentials

$$S(\boldsymbol{r}) = \Sigma_S(\boldsymbol{r}) + \tau_3 \Sigma_{\text{TS}}(\boldsymbol{r}), \tag{33}$$

$$V^\mu(\boldsymbol{r}) = \Sigma^\mu(\boldsymbol{r}) + \tau_3 \Sigma_{\text{TV}}^\mu(\boldsymbol{r}), \tag{34}$$

contain the nucleon isoscalar-scalar, isovector-scalar, isoscalar-vector, and isovector-vector self-energies defined by the following relations:

$$\Sigma_S = \alpha_S \rho_S + \beta_S \rho_S^2 + \gamma_S \rho_S^3 + \delta_S \triangle \rho_S, \tag{35}$$

$$\Sigma_{\text{TS}} = \alpha_{\text{TS}} \rho_{\text{TS}} + \delta_{\text{TS}} \triangle \rho_{\text{TS}}, \tag{36}$$

$$\Sigma^\mu = \alpha_V j^\mu + \gamma_V (j_\nu j^\nu) j^\mu + \delta_V \triangle j^\mu - e A^\mu \frac{1 - \tau_3}{2}, \tag{37}$$

$$\Sigma_{\text{TV}}^\mu = \alpha_{\text{TV}} j_{\text{TV}}^\mu + \delta_{\text{TV}} \triangle j_{\text{TV}}^\mu, \tag{38}$$

respectively. Because of charge conservation, only the third component of the isovector densities and currents contributes to the nucleon self-energies. In this work, we only consider even-even nuclei, i.e., time-reversal invariance is assumed, which implies that the spatial components of the single-nucleon currents vanish in the nuclear ground state.

The Dirac equation (32) is solved by expanding the nucleon spinors in the basis of a three-dimensional harmonic oscillator in Cartesian coordinates. In this way, both axial and triaxial nuclear shapes can be described. In addition, to reduce the computational task, it is assumed that the total densities are symmetric under reflections with respect to all three planes xy, xz, and yz. When combined with time-reversal invariance, this also implies that parity is conserved. Under these restrictions, we consider only even-multipole deformations, whereas solutions for odd multipoles vanish. The method of solution of the Dirac equation is described in more detail in Appendix A.

In addition to the self-consistent mean-field potential, for open-shell nuclei, pairing correlations have to be included in the energy functional. In this work, pairing is treated using the BCS formalism. Following the prescription from Ref. [43], we employ a δ force in the pairing channel, supplemented

with a smooth cutoff determined by a Fermi function in the single-particle energies. The pairing contribution to the total energy is given by

$$E_{\text{pair}}^{p(n)} = \int \mathcal{E}_{\text{pair}}^{p(n)}(\boldsymbol{r}) \, d\boldsymbol{r} = \frac{V_{p(n)}}{4} \int \kappa_{p(n)}^*(\boldsymbol{r}) \kappa_{p(n)}(\boldsymbol{r}) d\boldsymbol{r}, \tag{39}$$

for protons and neutrons, respectively. $\kappa_{p(n)}(\boldsymbol{r})$ denotes the local part of the pairing tensor, and $V_{p(n)}$ is the pairing strength parameter.

The center-of-mass correction is included by adding the expectation value

$$E_{\text{c.m.}} = -\frac{\langle \hat{P}_{\text{c.m.}}^2 \rangle}{2mA} \tag{40}$$

to the total energy. Finally, the expression for the total energy reads

$$E_{\text{tot}} = \int \left[\mathcal{E}_{\text{RMF}}(\boldsymbol{r}) + \mathcal{E}_{\text{pair}}^p(\boldsymbol{r}) + \mathcal{E}_{\text{pair}}^n(\boldsymbol{r}) \right] d\boldsymbol{r} + E_{\text{c.m.}}. \tag{41}$$

The entire map of the energy surface as a function of the quadrupole deformation is obtained by imposing constraints on the axial and triaxial mass quadrupole moments. The method of quadratic constraints uses an unrestricted variation of the function

$$\langle H \rangle + \sum_{\mu=0,2} C_{2\mu} (\langle \hat{Q}_{2\mu} \rangle - q_{2\mu})^2, \tag{42}$$

where $\langle H \rangle$ is the total energy, and $\langle \hat{Q}_{2\mu} \rangle$ denotes the expectation value of the mass quadrupole operator:

$$\hat{Q}_{20} = 2z^2 - x^2 - y^2 \quad \text{and} \quad \hat{Q}_{22} = x^2 - y^2. \tag{43}$$

Here $q_{2\mu}$ is the constrained value of the multipole moment, and $C_{2\mu}$ the corresponding stiffness constant [4].

The single-nucleon wave functions, energies, and occupation factors, generated from constrained self-consistent solutions of the RMF+BCS equations, provide the microscopic input for the parameters of the collective Hamiltonian.

The moments of inertia are calculated according to the Inglis-Belyaev formula [24,44]

$$\mathcal{I}_k = \sum_{i,j} \frac{(u_i v_j - v_i u_j)^2}{E_i + E_j} |\langle i | \hat{J}_k | j \rangle|^2 \quad k = 1, 2, 3, \tag{44}$$

where k denotes the axis of rotation, and the summation runs over the proton and neutron quasiparticle states. The quasiparticle energies E_i, occupation probabilities v_i, and single-nucleon wave functions ψ_i are determined by solutions of the constrained RMF+BCS equations. The mass parameters associated with the two quadrupole collective coordinates $q_0 = \langle \hat{Q}_{20} \rangle$ and $q_2 = \langle \hat{Q}_{22} \rangle$ are also calculated in the cranking approximation [18]

$$B_{\mu\nu}(q_0, q_2) = \frac{\hbar^2}{2} \left[\mathcal{M}_{(1)}^{-1} \mathcal{M}_{(3)} \mathcal{M}_{(1)}^{-1} \right]_{\mu\nu}, \tag{45}$$

with

$$\mathcal{M}_{(n),\mu\nu}(q_0, q_2) = \sum_{i,j} \frac{\langle i | \hat{Q}_{2\mu} | j \rangle \langle j | \hat{Q}_{2\nu} | i \rangle}{(E_i + E_j)^n} (u_i v_j + v_i u_j)^2. \tag{46}$$

The collective energy surface includes the energy of the zero-point motion, which has to be subtracted. The collective zero-point energy (ZPE) corresponds to a superposition of zero-point motion of individual nucleons in the single-nucleon potential. In the general case, the ZPE corrections on the potential energy surfaces depend on the deformation. The ZPE includes terms originating from the vibrational and rotational kinetic energy, and a contribution of potential energy

$$\Delta V(q_0, q_2) = \Delta V_{\text{vib}}(q_0, q_2) + \Delta V_{\text{rot}}(q_0, q_2) \\ + \Delta V_{\text{pot}}(q_0, q_2). \quad (47)$$

The latter is much smaller than the contribution of kinetic energy and is usually neglected [25]. Simple prescriptions for the calculation of vibrational and rotational ZPE have been derived in Ref. [18]. Both corrections are calculated in the cranking approximation, i.e., on the same level of approximation as the mass parameters and moments of inertia. The vibrational ZPE is given by the expression

$$\Delta V_{\text{vib}}(q_0, q_2) = \tfrac{1}{4} \operatorname{Tr} \left[\mathcal{M}_{(3)}^{-1} \mathcal{M}_{(2)} \right]. \quad (48)$$

The rotational ZPE is a sum of three terms:

$$\Delta V_{\text{rot}}(q_0, q_2) = \Delta V_{-2-2}(q_0, q_2) + \Delta V_{-1-1}(q_0, q_2) \\ + \Delta V_{11}(q_0, q_2), \quad (49)$$

with

$$\Delta V_{\mu\nu}(q_0, q_2) = \frac{1}{4} \frac{\mathcal{M}_{(2),\mu\nu}(q_0, q_2)}{\mathcal{M}_{(3),\mu\nu}(q_0, q_2)}. \quad (50)$$

The individual terms are calculated from Eqs. (50) and (46), with the intrinsic components of the quadrupole operator defined by

$$\hat{Q}_{21} = -2iyz, \quad \hat{Q}_{2-1} = -2xz, \quad \hat{Q}_{2-2} = 2ixy. \quad (51)$$

The potential V_{coll} in the collective Hamiltonian (12) is obtained by subtracting the ZPE corrections from the total mean-field energy defined in Eq. (41):

$$V_{\text{coll}}(q_0, q_2) = E_{\text{tot}}(q_0, q_2) - \Delta V_{\text{vib}}(q_0, q_2) - \Delta V_{\text{rot}}(q_0, q_2). \quad (52)$$

Detailed expressions for the parameters of the collective Hamiltonian are given in Appendixes B and C.

III. ILLUSTRATIVE CALCULATIONS: THE GADOLINIUM ISOTOPIC CHAIN

In this section, the new implementation is tested in a series of illustrative calculations of potential energy surfaces and the resulting collective excitation spectra of the chain of even-even Gd isotopes: $^{152-160}$Gd. The transition between different shapes, from the weakly deformed transitional ^{152}Gd to the well-deformed prolate ^{160}Gd, is illustrated in Fig. 1, where we plot the self-consistent RMF+BCS binding energy curves for the axially symmetric configurations as functions of the deformation parameter β. Negative values of β correspond
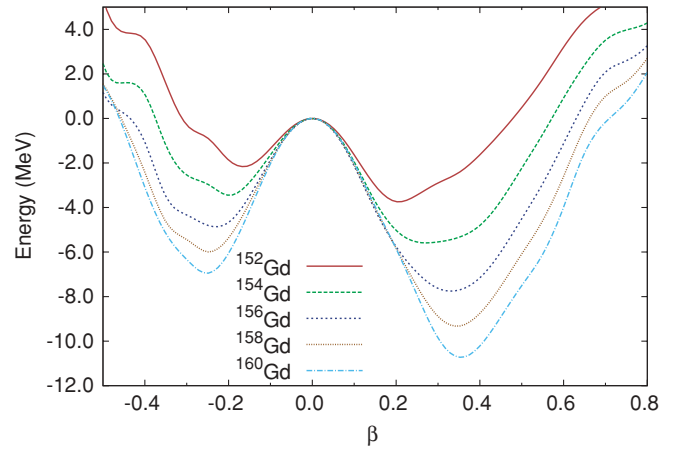

FIG. 1. (Color online) Self-consistent RMF+BCS binding energy curves of the $^{152-160}$Gd isotopes, as functions of the axial deformation parameter β. Negative values of β correspond to the ($\beta > 0$, $\gamma = 180°$) axis on the β-γ plane.

to the $\beta > 0$, $\gamma = 180°$ axis on the β-γ plane. ^{152}Gd is characterized by the coexistence of two weakly deformed prolate ($\beta \approx 0.2$) and oblate ($\beta \approx -0.2$) minima, with the prolate minimum ≈ 4 MeV below the spherical configuration. With the addition of more neutrons, the deformed minima become deeper and gradually shift to larger values of β. For ^{160}Gd, the constrained RMF+BCS calculation with the PC-F1 interaction predicts a pronounced prolate minimum at ($\beta \approx 0.35$), more than 10 MeV below the corresponding spherical configuration.

In Figs. 2–6 we display the self-consistent RMF+BCS triaxial quadrupole binding energy maps of $^{152-160}$Gd in the β-γ plane ($0 \leqslant \gamma \leqslant 60°$), obtained by imposing constraints on the expectation values of the quadrupole moments $\langle \hat{Q}_{20} \rangle$ and $\langle \hat{Q}_{22} \rangle$ [cf. Eq. (42)]. Filled circles denote absolute minima; all
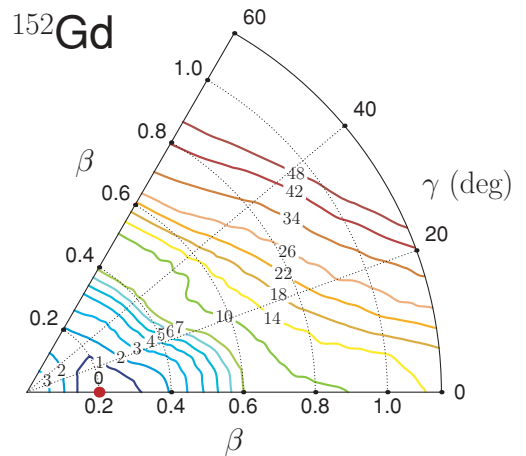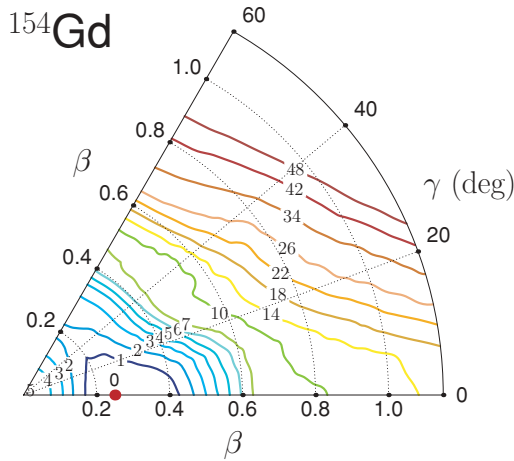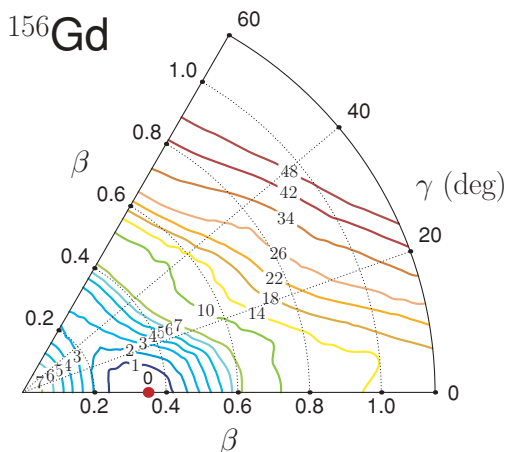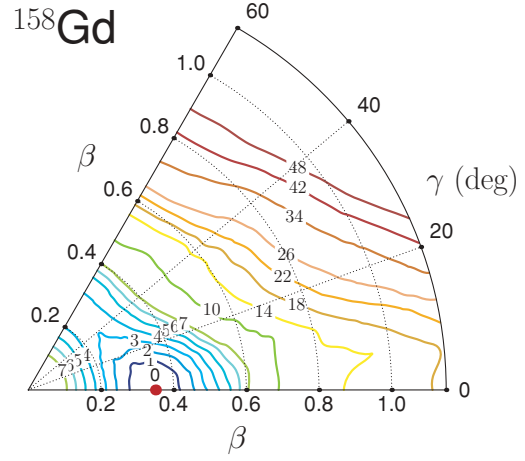

FIG. 2. (Color online) Self-consistent RMF+BCS triaxial quadrupole binding energy map of ^{152}Gd in the β-γ plane ($0 \leqslant \gamma \leqslant 60°$). All energies are normalized with respect to the binding energy of the absolute minimum (large red dot). The contours join points on the surface with the same energy (in MeV).

FIG. 3. (Color online) Same as Fig. 2, but for the nucleus ^{154}Gd.

FIG. 5. (Color online) Same as Fig. 2, but for the nucleus ^{158}Gd.
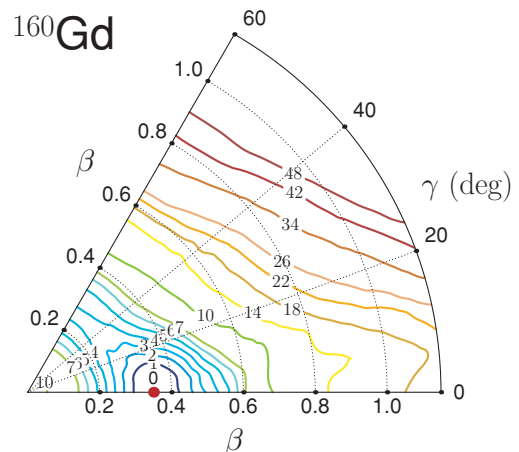
energies are normalized with respect to the binding energy of the absolute minimum. The contours join points with the same energy. The energy maps nicely illustrate the gradual increase of deformation of the prolate minimum with increasing number of neutrons. One notes, however, that the oblate minima shown in the axial plots in Fig. 1 are not true minima but rather saddle points in the β-γ plane.

Starting from constrained self-consistent solutions, i.e., using the single-particle wave functions, occupation probabilities, and quasiparticle energies that correspond to each point on the energy surfaces shown in Figs. 2–6, the parameters that determine the collective Hamiltonian, that is, the mass parameters $B_{\beta\beta}$, $B_{\beta\gamma}$, $B_{\gamma\gamma}$, three moments of inertia $\mathcal{I}_k$, as well as the zero-point energy corrections, are calculated as functions of the deformations β and γ. As an illustration, for ^{154}Gd the contour map of the inertia parameter B_x [cf. Eq. (B19)] is shown in Fig. 7, and the mass parameter $B_{\beta\beta}$ in Fig. 8. The inertia parameter decreases with the increase of the axial deformation β, but the dependence on γ is very weak. The mass parameters, on the other hand, display a pronounced dependence on both intrinsic deformations β and γ. We notice that $B_{\beta\beta}$ generally increases with the increase of γ

from prolate ($\gamma \approx 0°$) toward oblate ($\gamma \approx 60°$) configurations. The somewhat erratic behavior of $B_{\beta\beta}$, in particular, is mainly caused by the fluctuations of pairing correlations as function of β and γ [cf. Eq. (46) with its strong dependence on the quasiparticle energies]. This effect is illustrated in Figs. 9 and 10, where we plot the contour maps of the proton and neutron pairing energies, respectively, in the β-γ plane. The fluctuations of pairing energies reflect the underlying shell structure, and because pairing correlations are described in the BCS approximations, pairing is strongly reduced wherever the level density around the Fermi level is small. As a result, mass parameters are locally enhanced in regions of weak pairing.

Figure 11 displays the contour plot of the rotational zero-point energy correction [Eq. (49)] for ^{154}Gd. The rotational ZPE, of course, increases with the axial deformation β, but we also notice a pronounced dependence on γ. The ZPE corrections are of the order of several MeV even in the region close to the minimum and can, therefore, present a significant contribution to the potential of the collective Hamiltonian. This is illustrated for ^{154}Gd in Fig. 12, where we plot the potential V_{coll} [Eq. (52)] in the β-γ plane. When this plot is

FIG. 4. (Color online) Same as Fig. 2, but for the nucleus ^{156}Gd.

FIG. 6. (Color online) Same as Fig. 2, but for the nucleus ^{160}Gd.

FIG. 7. (Color online) Map of the Inglis-Belyaev inertia parameter B_x of ^{154}Gd in the β-γ plane ($0 \leqslant \gamma \leqslant 60°$).

compared with the total mean-field energy of Eq. (41) (cf. Fig. 3), one notes that the main effect of ZPE corrections is to shift the position of the minimum to a larger prolate deformation and to modify the shape of the potential around the minimum.

The diagonalization of the resulting Hamiltonian yields the excitation energies and the collective wave functions for each value of the total angular momentum and parity I^{π}. In addition to the yrast ground-state band, in deformed and transitional nuclei, excited states are usually also assigned to (quasi) β and γ bands. This is done according to the distribution of the angular-momentum projection K quantum number defined in Eq. (26). Excited states with predominant $K = 2$ components in the wave function are assigned to the γ band, whereas the β band comprises states above the yrast characterized by dominant $K = 0$ components. As an example, in Fig. 13 we display the PC-F1 excitation spectrum of ^{154}Gd, in comparison with available data [45]. The relative excitation energies within all three theoretical bands are scaled by the common factor of ≈ 0.69, determined in such a way that the calculated energy of the 2_1^+ state coincides with the experimental value. This leaves the bandheads of the γ and β bands unaltered and corresponds to an enhancement of the effective moment of inertia by $\approx 45\%$.

FIG. 9. (Color online) Proton pairing energy of ^{154}Gd in the β-γ plane ($0 \leqslant \gamma \leqslant 60°$). The contours join points on the surface with the same energy (in MeV).

FIG. 10. (Color online) Neutron pairing energy of ^{154}Gd in the β-γ plane ($0 \leqslant \gamma \leqslant 60°$). The contours join points on the surface with the same energy (in MeV).

FIG. 8. (Color online) Cranking mass parameter $B_{\beta\beta}$ of ^{154}Gd in the β-γ plane ($0 \leqslant \gamma \leqslant 60°$).

FIG. 11. (Color online) Rotational zero-point energy of ^{154}Gd in the β-γ plane ($0 \leqslant \gamma \leqslant 60°$).

FIG. 12. (Color online) Potential V_{coll} [Eq. (52)] of ^{154}Gd in the β-γ plane ($0 \leqslant \gamma \leqslant 60°$). The contours join points on the surface with the same energy (in MeV).

The scaling of the relative excitation energies is introduced because of the well-known fact that the Inglis-Belyaev (IB) formula (44) predicts effective moments of inertia that are considerably smaller than empirical values. More realistic values are only obtained if one uses the Thouless-Valatin (TV) formula [23], but this procedure is computationally much more demanding, and it has not been implemented in the current version of the model. Here we rather follow the prescription of Ref. [25] where, by comparing the TV and IB moments of inertia as functions of the axial deformation for superdeformed bands in the $A = 190$–198 mass region, it was shown that the Thouless-Valatin correction to the perturbative expression IB is almost independent of deformation and does not include significant new structures in the moments of inertia. It was thus suggested that the moments of inertia to be used in

the collective Hamiltonian can be simply related to the IB values through the minimal prescription $\mathcal{I}_k(q) = \mathcal{I}_k^{IB}(q)(1 + \alpha)$, where q denotes the generic deformation parameter, and α is a constant that can be determined in a comparison with data. The value of $\alpha \approx 0.45$ used for the excitation spectrum of ^{154}Gd is somewhat larger than the values determined in the mass $A = 190$–198 region [25].

When the IB effective moments of inertia are renormalized to the empirical values by scaling the relative excitation energies to reproduce the experimental position of the state 2_1^+, the resulting bands are in good agreement with data. This is illustrated in Figs. 14–16, where we plot the excitation energies with respect to bandheads, for the ground-state, γ, and β bands, respectively, in $^{152-160}$Gd. For each nucleus, the relative excitation energies within the three bands are scaled by a common factor, adjusted to the experimental energy of the 2_1^+ state, as explained above. These factors are rather similar for four isotopes: 0.69 for ^{154}Gd, 0.67 for ^{156}Gd, 0.69 for ^{158}Gd, and 0.72 for ^{160}Gd. An exception is the lightest Gd isotope considered here: ^{152}Gd, for which this factor is actually 1.08, i.e., the theoretical 2_1^+ state ($E_x = 0.318$ MeV) is slightly below the experimental 2_1^+ state ($E_x = 0.344$ MeV). However, as shown in Figs. 14–16, for this nucleus, the calculated ground-state band, as well as the (quasi) γ and β bands, do not follow very closely the experimental spectra. The deviation from the experimental trend at higher angular momenta can probably be explained by the fact that this is a weakly deformed transitional nucleus for which the assumption of a constant moment of inertia, implicit in the expression $\mathcal{I}_k(q) = \mathcal{I}_k^{IB}(q)(1 + \alpha)$, and of relatively pure β and γ bands, does not present a very good approximation.

The calculated β bands are compared with available data in Fig. 16. In comparison with the γ bands (cf. Fig. 15), the agreement with data is better in ^{152}Gd, but the deviation from experiment is more pronounced in ^{156}Gd. To understand
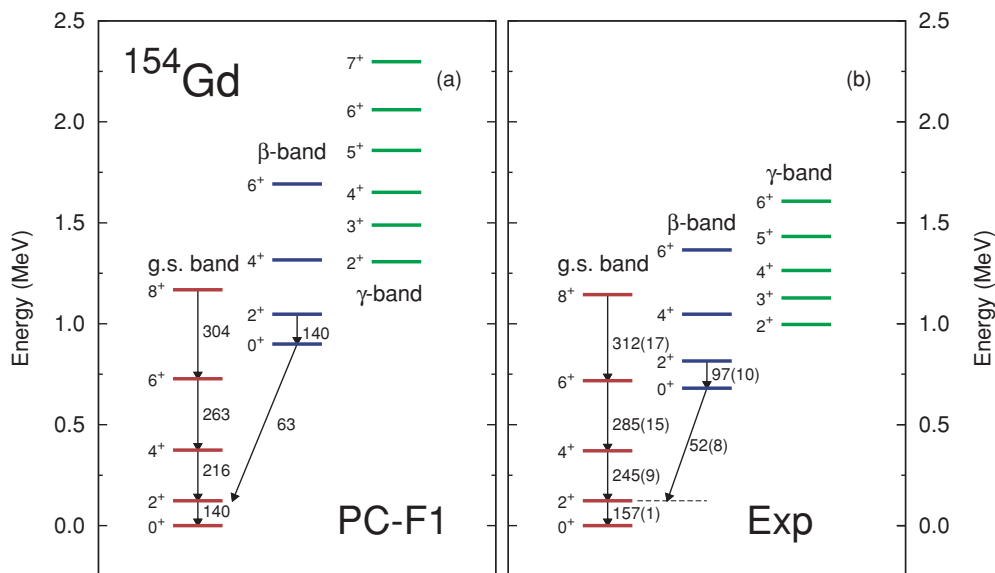

FIG. 13. (Color online) Level scheme of ^{154}Gd calculated with the PC-F1 relativistic density functional, in comparison with experimental data [45]. The relative excitation energies are scaled by the common factor ≈ 0.69, adjusted to the experimental energy of the state 2_1^+. The $B(E2)$ values are given in Weisskopf units.
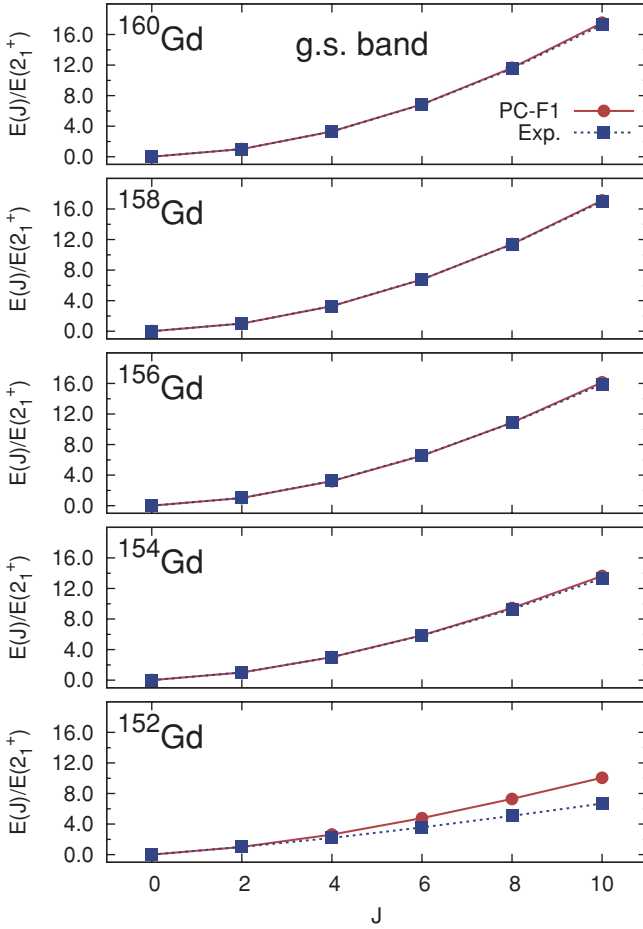
FIG. 14. (Color online) Relative ground-state band excitation energies in $^{152-160}$Gd. For each nucleus, the theoretical energies are scaled by a common factor, adjusted to the experimental energy of the 2_1^+ state.
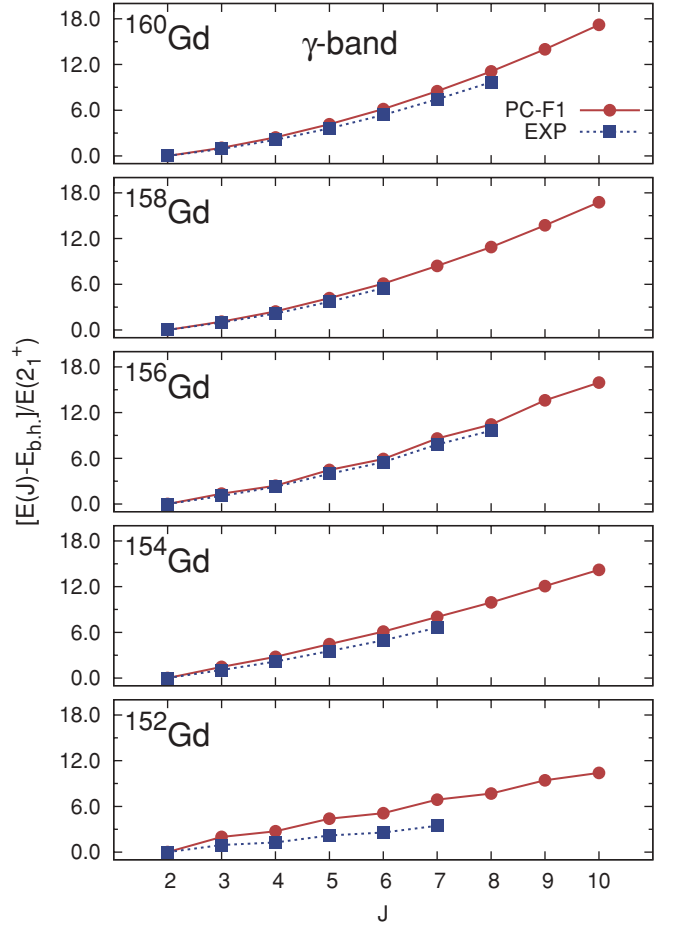

FIG. 15. (Color online) Comparison between the theoretical and experimental γ-band excitation energies for $^{152-160}$Gd. The scaling factors are the same as for the ground-state bands in Fig. 14.

in more detail the discrepancy between the calculated and empirical β and γ bands, we need to consider the distribution of the angular-momentum projection K quantum number [cf. Eq. (26)] in these bands. As explained above, the calculated second and third eigenstate for each angular momentum are assigned to either the β or γ band, on the basis of the predominant $K = 0$ or $K = 2$ components, respectively. The distributions of K components in the wave functions of the calculated second and third 2^+, 4^+, and 6^+ states are plotted in Figs. 17–19, respectively. In the case of ^{152}Gd, in particular, we find a pronounced mixing of the $K = 0$ or $K = 2$ components, and with increasing angular momentum, contributions of higher K components are present in the wave functions. This is consistent with the observation that ^{152}Gd is a transitional nucleus, and therefore excited states can be only approximately assigned to (quasi) β and γ bands. Increasing the neutron number toward heavier and more deformed Gd isotopes, the distributions of K components become sharp, and states can unambiguously be grouped into β and γ bands. This is, of course, characteristic for well-deformed nuclei. One exception, however, is the calculated spectrum of ^{156}Gd, where we find significant mixing of $K = 0$ and $K = 2$ components

in the wave functions of second and third 2^+, 4^+, and 6^+ states, as well as for higher angular momenta. The more pronounced mixing between the β and γ bands occurs because, in this particular isotope, the calculated second and third even-spin states are almost degenerate in energy, as shown in Fig. 20.

The level of K mixing is reflected in the staggering in energy between odd- and even-spin states in the (quasi) γ bands (cf. Fig. 15). The staggering can be quantified by considering the differential quantity [46]

$$
\begin{aligned}
&S(J) \\
&= \frac{\{E[J_\gamma^+] - E[(J-1)_\gamma^+]\} - \{E[(J-1)_\gamma^+] - E[(J-2)_\gamma^+]\}}{E[2_1^+]},
\end{aligned}
$$
(53)

which measures the displacement of the $(J-1)_\gamma^+$ level relative to the average of its neighbors, J_γ^+ and $(J-2)_\gamma^+$, normalized to the energy of the first excited state of the ground-state band, 2_1^+. Because of its differential form, $S(J)$ is very sensitive to structural changes. For an axially symmetric rotor, $S(J)$ is, of course, constant. In a nucleus with a deformed γ-soft potential, $S(J)$ oscillates between negative values for even-spin states
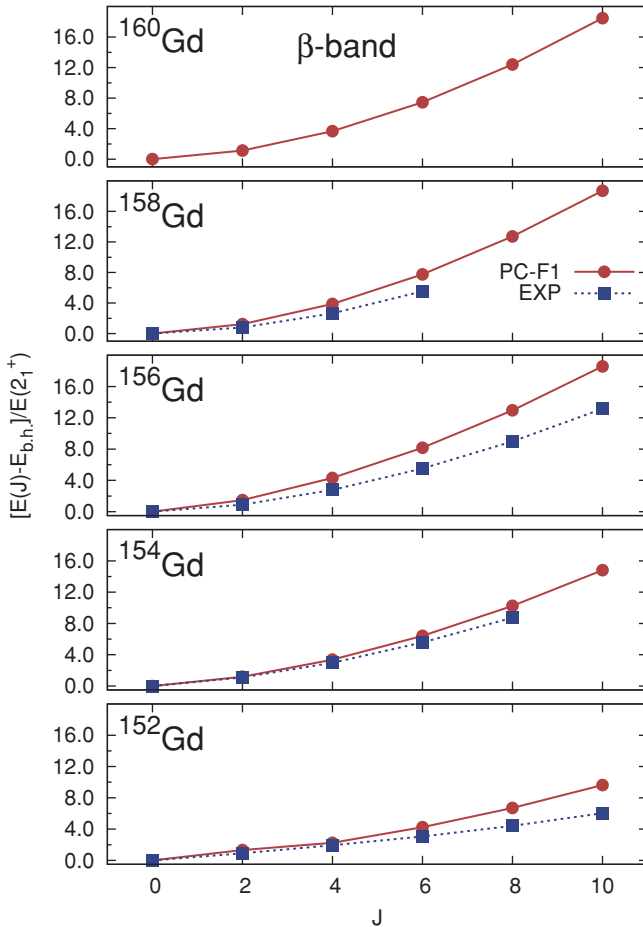
FIG. 16. (Color online) Same as in Fig. 15, but for the β bands in $^{152-160}$Gd. The scaling factors are the same as for the ground-state bands in Fig. 14.

TABLE I. Average values of the deformation parameters β and γ [cf. Eqs. (24) and (25)] for the calculated first, second, and third 2^+, 4^+, and 6^+ states in $^{152-160}$Gd. γ is in degrees.

State		2^+		4^+		6^+	
		$\langle\beta\rangle$	$\langle\gamma\rangle$	$\langle\beta\rangle$	$\langle\gamma\rangle$	$\langle\beta\rangle$	$\langle\gamma\rangle$
^{152}Gd	J_1^+	0.24	17.0	0.26	15.3	0.28	13.7
	J_2^+	0.26	19.0	0.31	13.9	0.32	12.8
	J_3^+	0.29	16.3	0.28	20.5	0.30	20.1
^{154}Gd	J_1^+	0.31	12.8	0.32	12.0	0.33	11.3
	J_2^+	0.33	12.8	0.33	12.4	0.34	12.2
	J_3^+	0.29	19.8	0.32	17.6	0.34	16.2
^{156}Gd	J_1^+	0.34	11.3	0.35	11.0	0.36	10.6
	J_2^+	0.34	13.0	0.34	14.0	0.35	13.6
	J_3^+	0.35	13.0	0.36	12.5	0.37	12.0
^{158}Gd	J_1^+	0.36	10.8	0.36	10.6	0.36	10.5
	J_2^+	0.36	14.3	0.36	13.8	0.37	13.4
	J_3^+	0.36	11.0	0.37	10.7	0.38	10.4
^{160}Gd	J_1^+	0.36	10.3	0.37	10.2	0.37	10.1
	J_2^+	0.37	13.4	0.37	13.2	0.37	12.9
	J_3^+	0.38	10.3	0.38	10.0	0.39	9.8

and positive values for odd-spin states, with the magnitude slowly increasing with spin. For a triaxial potential, the level clustering in the (quasi) γ band is opposite, and $S(J)$ oscillates between positive values for even-spin states and negative values for odd-spin states. In this case, the magnitude of $S(J)$ increases more rapidly with spin, as compared to the γ-soft potential. In a recent study of staggering of γ-band energies and the transition between different structural symmetries in nuclei [47], the experimental energy staggering in γ bands of several isotopic chains was investigated as a signature for the γ dependence of the potential. In Fig. 21, we plot the staggering in the γ band for the chain of Gd isotopes, calculated with the PC-F1 relativistic density functional. One notices how the pronounced K mixing in ^{152}Gd and ^{156}Gd (cf. Figs. 17–19) leads to the strong staggering observed in the corresponding (quasi) γ bands. The calculation reproduces both the empirical oscillatory behavior and, with the exception of low-spin states in ^{156}Gd, also the magnitude of $S(J)$. Starting from the γ-soft ^{152}Gd (negative values for even-spin states and positive values for odd-spin states), $S(J)$ evolves toward the axially symmetric rotor limit [$S(J) = 0.33$] in ^{158}Gd and ^{160}Gd.

The assignment of even-spin states above the yrast either to the β or γ bands, on the basis of the predominant $K =$ 0 or $K = 2$ components (Figs. 17–19) and the level of K mixing inferred from the differential quantity $S(J)$ of Eq. (53) (Fig. 21), has a correspondence in the calculated average values of the deformation parameters β and γ [cf. Eqs. (24) and (25)]. In Table I, we collect the average β and γ deformations for the calculated first, second, and third 2^+, 4^+, and 6^+ states in $^{152-160}$Gd. For those nuclei where the K mixing is weak [sharp distribution of K components in Figs. 17–19, weak staggering of $S(J)$ in Fig. 21], i.e., ^{154}Gd, ^{158}Gd, and ^{160}Gd, the average values of the deformation parameters are almost identical for states belonging to the ground-state band and those assigned to the β band. States assigned to the γ band ($K = 2$) are consistently characterized by larger average values of the angle γ. This distinction does not appear in the spectra of the two nuclei for which the model predicts pronounced K mixing: ^{152}Gd and ^{156}Gd.

An important advantage of using structure models based on self-consistent mean-field single-particle solutions is that physical observables, such as transition probabilities and spectroscopic quadrupole moments, are calculated in the full configuration space, and there is no need for effective charges. Using the bare value of the proton charge in the electric quadrupole operator $\hat{\mathcal{M}}(E2)$, the transition probabilities between eigenvectors of the collective Hamiltonian can be directly compared with data. In addition to the calculated energy spectrum of ^{154}Gd, in Fig. 13 we have also compared the resulting $B(E2)$ values (in Weisskopf units) for transitions within the ground-state band, and the transitions $2_\beta^+ \to 0_\beta^+$ and $0_\beta^+ \to 2_{g.s.}^+$, with available experimental values. The agreement between theoretical $B(E2)$ values and data is very good, especially considering that the calculation of
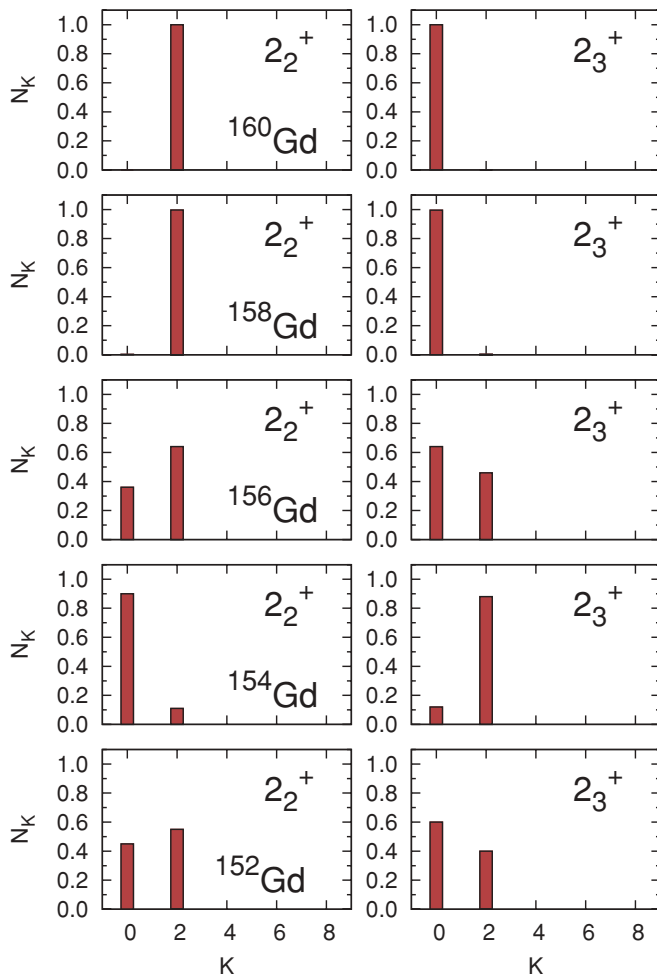
FIG. 17. (Color online) Distribution of the K components (projection of the angular momentum on the body-fixed symmetry axis) in the collective wave functions for the states 2_2^+ and 2_3^+.

FIG. 18. (Color online) Same as Fig. 17, but for the states 4_2^+ and 4_3^+.

transition probabilities is completely parameter-free. We also notice the remarkable prediction for the interband transition $0_\beta^+ \rightarrow 2_{g.s.}^+$, in excellent agreement with experiment. Finally, in Fig. 22, we plot the calculated $B(E2)$ values (in Weisskopf units) for the ground-state band transitions $J_1^+ \rightarrow (J-2)_1^+$ in $^{152-160}$Gd, together with the available experimental values. The model clearly reproduces the empirical trend of ground-state band transitions in Gd isotopes; and, except perhaps for the transitional nucleus ^{152}Gd, the theoretical predictions are in excellent agreement with data even for higher angular-momentum states.

IV. SUMMARY AND OUTLOOK

To describe complex excitation patterns and electromagnetic transition rates associated with the evolution of shell structures starting from stable nuclei and extending toward regions of exotic short-lived systems far from β stability, nuclear structure methods must be developed that are based on a universal microscopic framework. Properties of a vast majority of nuclides with a large number of valence nucleons are best described by nuclear energy density functionals. However, for a quantitative description of energy spectra and transition probabilities, one must be able to go beyond the lowest order in which the EDFs are implemented—the mean-field approximation—and systematically include correlations related to the restoration of broken symmetries and to fluctuations of collective variables. In the framework of nonrelativistic EDFs, several models have been developed in recent years that use the generator coordinate method (GCM) to perform configuration mixing calculations with angular-momentum and particle-number projected mean-field (SR EDF) states. In most applications, the calculations have been restricted to axially symmetric, parity-conserving configurations.

In a recent series of papers, of which the present is the third part, we have extended the relativistic EDFs to include symmetry restoration and fluctuations of quadrupole deformations. While in the first two parts, the GCM was used in configuration mixing calculations with axially symmetric relativistic wave functions, this work has been focused on the description of general triaxial shapes. We have developed a new implementation for the solution of the eigenvalue
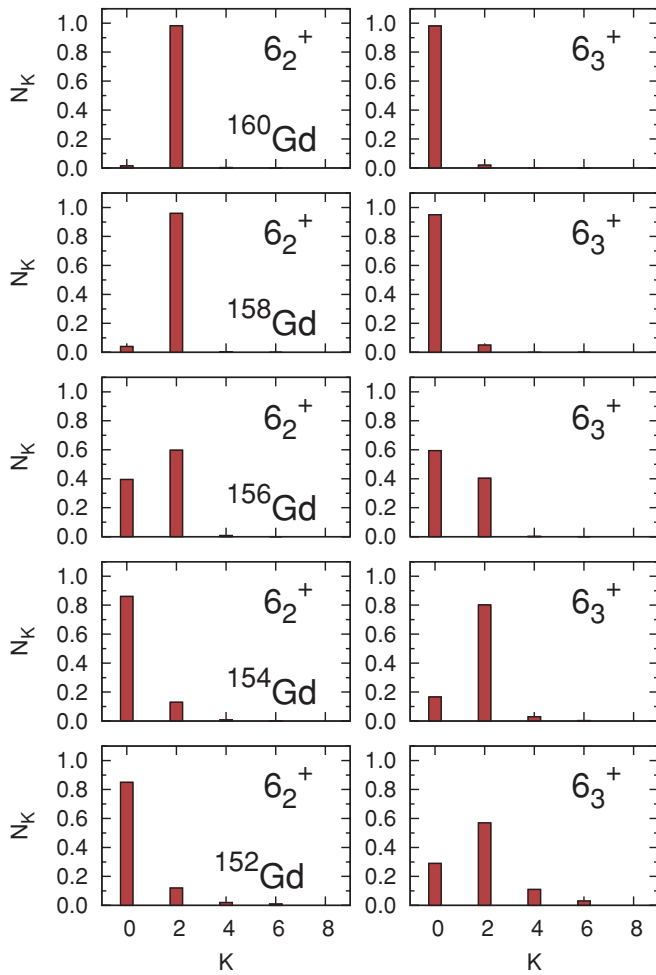
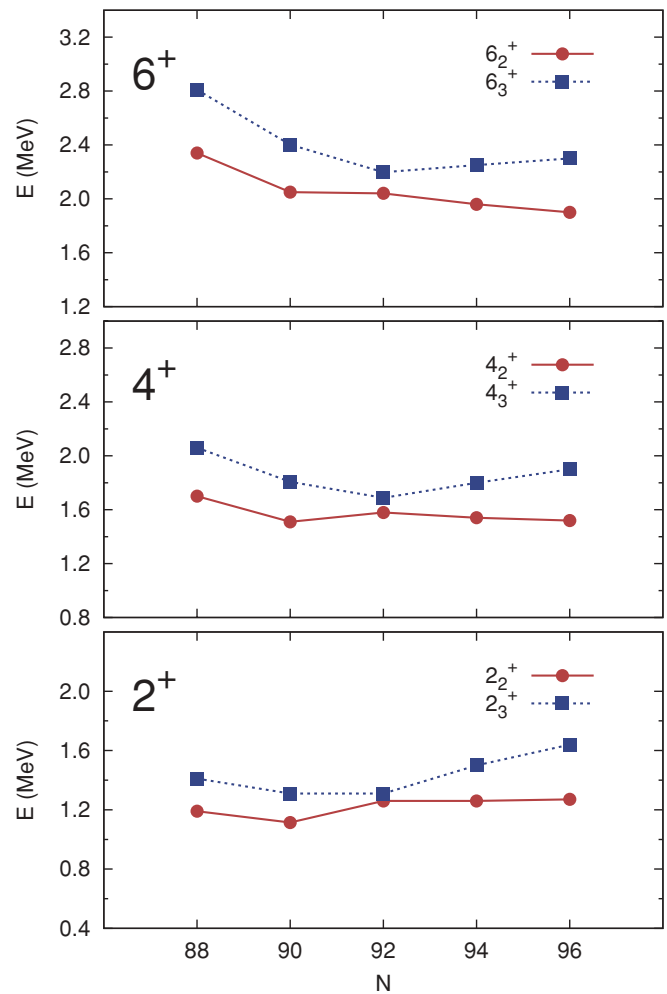FIG. 19. (Color online) Same as Fig. 17, but for the states 6_2^+ and 6_3^+.

FIG. 20. (Color online) Excitation energies of the second and third states 2^+, 4^+, and 6^+ in the Gd isotopic chain, as functions of the neutron number.

problem of a five-dimensional collective Hamiltonian for quadrupole vibrational and rotational degrees of freedom, with parameters determined by constrained self-consistent relativistic mean-field calculations for triaxial shapes. In addition to the self-consistent mean-field potential of the PC-F1 relativistic density functional in the particle-hole channel, for open-shell nuclei, pairing correlations are included in the BCS approximation. The resulting single-nucleon wave functions, energies and occupation factors, as functions of the quadrupole deformations, provide the microscopic input for the parameters of the collective Hamiltonian: three mass parameters $B_{\beta\beta}$, $B_{\beta\gamma}$, $B_{\gamma\gamma}$, three moments of inertia $\mathcal{I}_k$, and the collective potential including zero-point vibrational and rotational energy corrections. The moments of inertia are calculated using the Inglis-Belyaev formula, and the mass parameters associated with the quadrupole collective coordinates are determined in the cranking approximation. An extensive test has been carried out in calculations of potential energy surfaces, and the resulting collective excitation spectra and transition probabilities, for the chain of even-even gadolinium isotopes. Results for excitation energies in ground-state and (quasi) β and γ bands, and the corresponding interband and intraband transition probabilities have been compared with available data on even-even Gd isotopes: $^{152-160}$Gd.

Some obvious improvements need to be implemented in the model. For instance, because the Inglis-Belyaev formula gives effective moments of inertia that are lower than empirical values, all the calculated relative excitation energies in $^{152-160}$Gd have to be scaled with respect to the experimental energy of the 2_1^+ states. The moments of inertia can be improved by including the Thouless-Valatin dynamical rearrangement contributions. For the rotational degrees of freedom for which the collective momenta are known, the inertia parameters can be obtained from the solutions of cranked RMF equations. For the deformation coordinates q_0 and q_2, the situation is more complicated, because the corresponding momentum operators $\hat{P}_0$ and $\hat{P}_2$ have to be calculated from the solution of Thouless-Valatin equations [23] at each deformation point. Because cranking breaks time-reversal symmetry, in both cases the inclusion of pairing correlations necessitates the extension of the model from the simple RMF+BCS to the full relativistic Hartree-Bogoliubov framework [2].
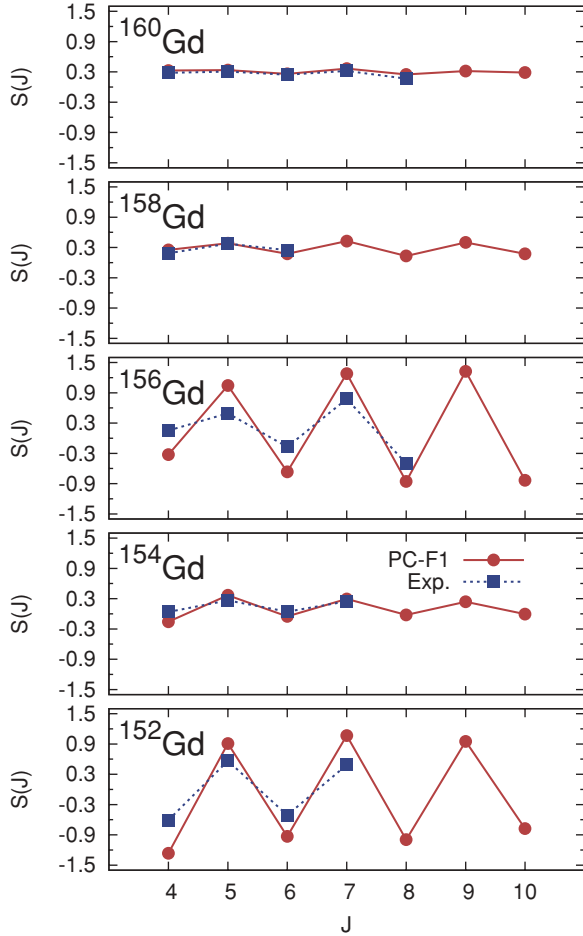
FIG. 21. (Color online) Staggering $S(J)$ [Eq. (53)] in the γ bands of $^{152-160}$Gd. Theoretical predictions are compared with experimental values.
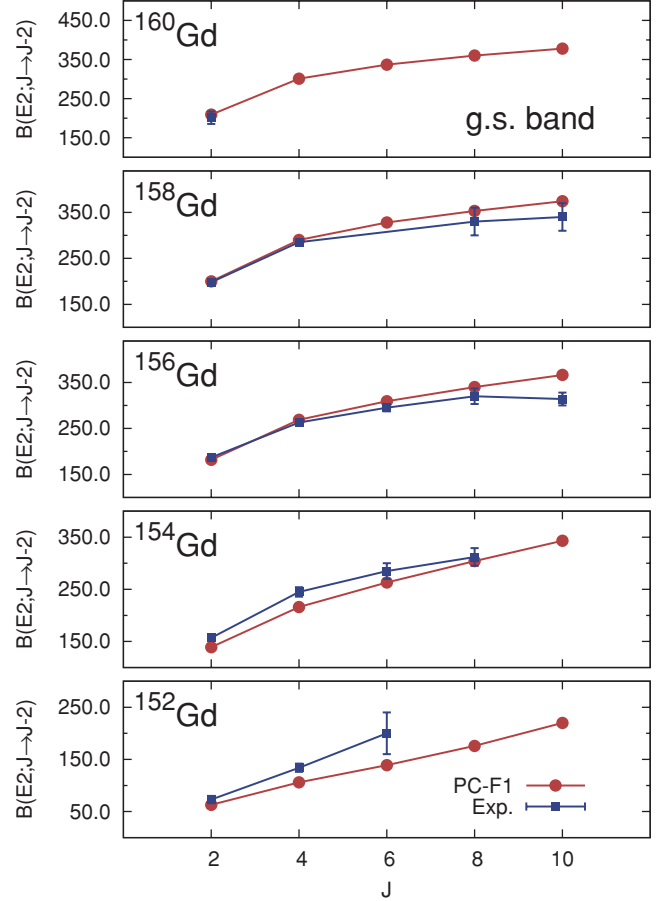

FIG. 22. (Color online) $B(E2)$ values (in Weisskopf units) for the ground-state band transitions $J_1^+ \rightarrow (J-2)_1^+$ in $^{152-160}$Gd. Theoretical values calculated with the PC-F1 relativistic density functional are compared with data.

APPENDIX A: THREE-DIMENSIONAL SOLUTION OF THE DIRAC EQUATION

To solve the Dirac equation (32) for triaxially deformed potentials, the single-nucleon spinors are expanded in the basis of eigenfunctions of a three-dimensional harmonic oscillator (HO) in Cartesian coordinates [48–51]. In one dimension,

$$\phi_{n_\mu}(x_\mu) = b_\mu^{-1/2} H_{n_\mu}(\xi_\mu) e^{-\xi_\mu^2/2} \quad (\mu \equiv x, y, z), \quad \text{(A1)}$$

$\xi_\mu \equiv x_\mu/b_\mu$, and the oscillator length is defined as

$$b_\mu = \sqrt{\frac{\hbar}{m\omega_\mu}}. \quad \text{(A2)}$$

$H_n(\xi)$ denotes the normalized Hermite polynomials

$$\int_{-\infty}^{\infty} H_n(\xi) H_{n'}(\xi) e^{-\xi^2} d\xi = \delta_{nn'}. \quad \text{(A3)}$$

The basis state can be defined as the product of three HO wave functions (one for each dimension) and the spinor:

$$\Phi_\alpha(\mathbf{r}; m_s) = \phi_{n_x}(\xi_x) \phi_{n_y}(\xi_y) \phi_{n_z}(\xi_z) \chi_{m_s}, \quad \text{(A4)}$$

where the notation is $\alpha \equiv \{n_x, n_y, n_z\}$. It will be more convenient to use the eigenstates of the x-simplex operator defined by the relation

$$\hat{S}_x = \hat{P} e^{-i\pi J_x}, \quad \text{(A5)}$$

where $\hat{P}$ denotes the parity operator. It is easily verified that the x-simplex operator acting on the state $\Phi_\alpha(\mathbf{r}; m_s)$ leads to

$$\hat{S}_x \Phi_\alpha(\mathbf{r}; m_s) = -i(-1)^{n_x} \Phi_\alpha(x, y, z; -m_s). \quad \text{(A6)}$$

The eigenstates of the x-simplex operator with positive and negative eigenvalues read

$$\Phi_\alpha(\mathbf{r}; +) = \phi_{n_x}(x)\phi_{n_y}(y)\phi_{n_z}(z)\frac{i^{n_y}}{\sqrt{2}}[\chi_+ - (-1)^{n_x}\chi_-], \quad \text{(A7)}$$

$$\Phi_\alpha(\mathbf{r}; -) = \phi_{n_x}(x)\phi_{n_y}(y)\phi_{n_z}(z)$$
$$\times \frac{i^{n_y}}{\sqrt{2}}(-1)^{n_x+n_y+1}[\chi_+ + (-1)^{n_x}\chi_-]. \quad \text{(A8)}$$

For the Dirac spinor with positive simplex eigenvalue, the large component corresponds to positive, and the small component to negative eigenvalues

$$\psi_i(\mathbf{r}, +) = \begin{pmatrix} f_i(\mathbf{r}, +) \\ i g_i(\mathbf{r}, -) \end{pmatrix}. \quad \text{(A9)}$$

The large and small component are expanded in terms of the basis states (A7) and (A8) to

$$f_i(\mathbf{r}; +) = \sum_\alpha^{\alpha_{\max}} f_i^\alpha \Phi_\alpha(\mathbf{r}; +)$$

and

$$g_i(\mathbf{r}; -) = \sum_{\tilde\alpha}^{\tilde\alpha_{\max}} g_i^{\tilde\alpha} \Phi_{\tilde\alpha}(\mathbf{r}; -). \quad \text{(A10)}$$

To avoid the occurrence of spurious states, $\alpha_{\max}$ and $\tilde\alpha_{\max}$ are chosen in such a way that the corresponding major quantum numbers $N = n_x + n_y + n_z$ are not larger than some arbitrary N_F for the expansion of large components, and not larger than $N_F + 1$ for the expansion of small components [52]. The single-nucleon Dirac equation

$$\begin{pmatrix} V + m^* & \boldsymbol{\sigma} \cdot \boldsymbol{\nabla} \\ -\boldsymbol{\sigma} \cdot \boldsymbol{\nabla} & V - m^* \end{pmatrix} \begin{pmatrix} f_i(\mathbf{r}; +) \\ g_i(\mathbf{r}; -) \end{pmatrix} = \epsilon_i \begin{pmatrix} f_i(\mathbf{r}; +) \\ g_i(\mathbf{r}; -) \end{pmatrix}, \quad \text{(A11)}$$

with the effective nucleon mass $m^* = m + S$, reduces to a symmetric matrix eigenvalue problem

$$\begin{pmatrix} \mathcal{A}_{\alpha\alpha'} & \mathcal{B}_{\alpha\tilde\alpha'} \\ \mathcal{B}_{\tilde\alpha\alpha'} & \mathcal{C}_{\tilde\alpha\tilde\alpha'} \end{pmatrix} \begin{pmatrix} f_i^{\alpha'} \\ g_i^{\tilde\alpha'} \end{pmatrix} = \epsilon_i \begin{pmatrix} f_i^{\alpha'} \\ g_i^{\tilde\alpha'} \end{pmatrix}, \quad \text{(A12)}$$

of dimension $\alpha_{\max} + \tilde\alpha_{\max}$.

The time-reversal operator $\hat{T} = -i\sigma_y \hat{K}$ exchanges the simplex eigenvalues

$$\hat{T}\Phi_\alpha(\mathbf{r}; +) = -\Phi_\alpha(\mathbf{r}; -)$$

and

$$\hat{T}\Phi_\alpha(\mathbf{r}; -) = \Phi_\alpha(\mathbf{r}; +), \quad \text{(A13)}$$

and, thus, when acting on the Dirac spinors,

$$\hat{T}\psi_i(\mathbf{r}; +) = \hat{T}\begin{pmatrix} f_i(\mathbf{r}; +) \\ i g_i(\mathbf{r}; -) \end{pmatrix} = \begin{pmatrix} \hat{T}f_i(\mathbf{r}; +) \\ -i\hat{T}g_i(\mathbf{r}; -) \end{pmatrix}$$
$$= \begin{pmatrix} -f_i(\mathbf{r}; -) \\ -i g_i(\mathbf{r}; +) \end{pmatrix} = -\psi_i(\mathbf{r}; -). \quad \text{(A14)}$$

Time-reversed single-particle states correspond to opposite simplex eigenvalues. Because of time-reversal invariance, for each solution of the Dirac equation (A11) with positive simplex eigenvalue $\psi_i(\mathbf{r}; +)$, there exists a degenerate time-reversed solution with negative simplex eigenvalue $\psi_i(\mathbf{r}; -)$. Both

solutions contribute equally to the densities, and in practice only the Dirac equation for positive simplex eigenstates is solved.

In the current implementation of the model, parity is also imposed as a conserved symmetry. This means that the basis states split into two parity blocks, which can be diagonalized separately. In addition, we require that the densities are symmetric under reflections with respect to the yz, xz, and xy planes.

$$\rho_{s,v}(x, y, z) = \rho_{s,v}(-x, y, z) = \rho_{s,v}(x, -y, z)$$
$$= \rho_{s,v}(x, y, -z). \quad \text{(A15)}$$

The symmetries of the scalar and vector densities are, of course, fulfilled by the corresponding self-consistent scalar and vector potentials:

$$S(x, y, z) = S(-x, y, z) = S(x, -y, z) = S(x, y, -z), \quad \text{(A16)}$$

$$V(x, y, z) = V(-x, y, z) = V(x, -y, z) = V(x, y, -z). \quad \text{(A17)}$$

The self-consistent symmetries (A16) and (A17) simplify the evaluation of the matrix elements $\mathcal{A}_{\alpha\alpha'}$ and $\mathcal{C}_{\tilde\alpha\tilde\alpha'}$. First, the symmetry under reflections with respect to the xy, yz, and xz planes means that we need to calculate only matrix elements between states ϕ_α and $\phi_{\alpha'}$ for which

$$(-1)^{n_x} = (-1)^{n'_x}, \quad (-1)^{n_y} = (-1)^{n'_y},$$

and

$$(-1)^{n_z} = (-1)^{n'_z}. \quad \text{(A18)}$$

Furthermore, three-dimensional integrals reduce to the octant $x, y, z \geqslant 0$. The matrix elements of the vector and scalar potentials read

$$\mathcal{A}_{\alpha\alpha'} = \langle\alpha; +|m^* + V|\alpha'; +\rangle$$
$$= 8(-1)^{(n_y - n'_y)/2} \int_0^\infty \int_0^\infty \int_0^\infty \phi_{n_x}(x)\phi_{n_y}(y)\phi_{n_z}(z)$$
$$\times (V + m^*)\phi_{n'_x}(x)\phi_{n'_y}(y)\phi_{n'_z}(z)\, dV, \quad \text{(A19)}$$

$$\mathcal{C}_{\tilde\alpha\tilde\alpha'} = \langle\tilde\alpha; -|V - m^*|\tilde\alpha'; -\rangle$$
$$= 8(-1)^{(n_y - n'_y)/2} \int_0^\infty \int_0^\infty \int_0^\infty \phi_{n_x}(x)\phi_{n_y}(y)\phi_{n_z}(z)$$
$$\times (V - m^*)\phi_{n'_x}(x)\phi_{n'_y}(y)\phi_{n'_z}(z)\, dV. \quad \text{(A20)}$$

Note that the condition (A18) means that the difference $(n_y - n'_y)$ must be even, hence the matrix elements (A19) and (A20) are real.

The matrix elements of the kinetic energy term $\mathcal{B}_{\alpha\tilde\alpha'}$ can be calculated analytically using the expression

$$\partial_\mu \phi_{n_\mu}(x_\mu) = \frac{1}{\sqrt{2}b_\mu}\left[-\sqrt{n_\mu + 1}\phi_{n_\mu+1}(x_\mu) + \sqrt{n_\mu}\phi_{n_\mu-1}(x_\mu)\right], \quad \text{(A21)}$$

together with the orthogonality relation (A3). The operator $\boldsymbol{\sigma} \cdot \boldsymbol{\nabla}$ consists of three terms:

$$\mathcal{B}_{\alpha\tilde\alpha'} = \langle\alpha; +| - \sigma_x \partial_x - \sigma_y \partial_y - \sigma_z \partial_z|\tilde\alpha'; -\rangle$$
$$= \mathcal{B}_{\alpha\tilde\alpha'}^x + \mathcal{B}_{\alpha\tilde\alpha'}^y + \mathcal{B}_{\alpha\tilde\alpha'}^z, \quad \text{(A22)}$$

and the corresponding matrix elements are calculated from

$$
\mathcal{B}^x_{\alpha\tilde{\alpha}'} = (-1)^{n_y} \delta_{n_y n'_y} \delta_{n_z n'_z} \frac{1}{\sqrt{2}b_x}
$$
$$
\times \left[-\sqrt{n'_x + 1}\delta_{n_x n'_x+1} + \sqrt{n'_x}\delta_{n_x n'_x-1} \right], \quad \text{(A23)}
$$

$$
\mathcal{B}^y_{\alpha\tilde{\alpha}'} = (-1)^{n'_y} \delta_{n_x n'_x} \delta_{n_z n'_z} \frac{1}{\sqrt{2}b_y}
$$
$$
\times \left[\sqrt{n'_y + 1}\delta_{n_y n'_y+1} + \sqrt{n'_y}\delta_{n_y n'_y-1} \right], \quad \text{(A24)}
$$

$$
\mathcal{B}^z_{\alpha\tilde{\alpha}'} = (-1)^{n'_x+n'_y+1} \delta_{n_x n'_x} \delta_{n_y n'_y} \frac{1}{\sqrt{2}b_z}
$$
$$
\times \left[-\sqrt{n'_z + 1}\delta_{n_z n'_z+1} + \sqrt{n'_z}\delta_{n_z n'_z-1} \right]. \quad \text{(A25)}
$$

The set of self-consistent solutions of the single-nucleon Dirac equation determines the scalar and vector densities:

$$
\rho_v(\mathbf{r}) = 2 \sum_i v_i^2 \psi_i^\dagger(\mathbf{r};+)\psi_i(\mathbf{r};+), \quad \text{(A26)}
$$

$$
\rho_s(\mathbf{r}) = 2 \sum_i v_i^2 \psi_i^\dagger(\mathbf{r};+)\beta\psi_i(\mathbf{r};+). \quad \text{(A27)}
$$

Because of time-reversal symmetry, the summation is over positive simplex solutions. To calculate densities in coordinate space, one needs explicit expressions for the products of basis states:

$$
\phi_\alpha^\dagger(\mathbf{r};+)\phi_{\alpha'}(\mathbf{r};+) = (-1)^{(n'_y-n_y)/2}\phi_{n_x}(x)\phi_{n'_x}(x)\phi_{n_y}
$$
$$
\times(y)\phi_{n'_y}(y)\phi_{n_z}(z)\phi_{n'_z}(z), \quad \text{(A28)}
$$

$$
\phi_\alpha^\dagger(\mathbf{r};-)\phi_{\alpha'}(\mathbf{r};-) = (-1)^{(n_y-n'_y)/2}\phi_{n_x}(x)\phi_{n'_x}(x)\phi_{n_y}
$$
$$
\times(y)\phi_{n'_y}(y)\phi_{n_z}(z)\phi_{n'_z}(z). \quad \text{(A29)}
$$

Note that the symmetry requirement in Eq. (A15) imposes the condition (A18), and again the difference $(n_y - n'_y)$ is even, so the contributions (A28) and (A29) to the densities are both real.

APPENDIX B: MOMENTS OF INERTIA

The basic ingredient of the Inglis-Belyaev formula for the moments of inertia Eq. (44) are the matrix elements of the angular-momentum operators in the simplex basis (A7) and (A8). Here we present in detail the calculation of the matrix element of the $\hat{J}_x$ component between basis states with positive simplex eigenvalue

$$
\langle \alpha; +|\hat{J}_x|\alpha'; +\rangle. \quad \text{(B1)}
$$

For the other matrix elements, only the final expressions will be listed.

The x component of the total angular-momentum operator is the sum of the spin and the spatial contributions:

$$
\hat{J}_x = \frac{\hbar}{2}\hat{\sigma}_x + \hat{L}_x = \frac{\hbar}{2}\hat{\sigma}_x - i\hbar(y\partial_z - z\partial_y). \quad \text{(B2)}
$$

The spatial parts of the basis states are unaffected by the $\hat{\sigma}_x$ operator, thus generating the product of Kronecker δ symbols

$\delta_{n_x,n'_x}\delta_{n_y,n'_y}\delta_{n_z,n'_z}$. The contribution from the spin factors of the basis states is given by

$$
[\chi_+^\dagger - (-1)^{n_x}\chi_-^\dagger]\hat{\sigma}_x[\chi_+ - (-1)^{n_x}\chi_-]
$$
$$
= (-1)^{n_x+1} + (-1)^{n'_x+1}, \quad \text{(B3)}
$$

and the spin matrix element reads

$$
\frac{\hbar}{2}\langle \alpha;+|\hat{\sigma}_x|\alpha';+\rangle = \frac{\hbar}{2}\delta_{n_x,n'_x}\delta_{n_y,n'_y}\delta_{n_z,n'_z}(-1)^{n_x+1}. \quad \text{(B4)}
$$

Next, the contribution from the operator $\hat{L}_x$ is calculated

$$
\langle \alpha;+|\hat{L}_x|\alpha';+\rangle = -i\hbar\langle \alpha;+|y\partial_z - z\partial_y|\alpha';+\rangle. \quad \text{(B5)}
$$

The spin factors of the basis states are not affected by the $\hat{L}_x$ operator:

$$
[\chi_+^\dagger - (-1)^{n_x}\chi_-^\dagger][\chi_+ - (-1)^{n_x}\chi_-] = 1 + (-1)^{n_x+n'_x}. \quad \text{(B6)}
$$

To calculate the matrix elements of Eq. (B5), the following relations are used:

$$
x_\mu\phi_{n_\mu} = \frac{b_\mu}{\sqrt{2}}\left[\sqrt{n_\mu + 1}\phi_{n_\mu+1}(x_\mu) + \sqrt{n_\mu}\phi_{n_\mu-1}(x_\mu)\right],
$$
$$
\text{(B7)}
$$

$$
\partial_\mu\phi_{n_\mu}(x_\mu) = \frac{1}{\sqrt{2}b_\mu}\left[-\sqrt{n_\mu + 1}\phi_{n_\mu+1}(x_\mu)\right.
$$
$$
\left. + \sqrt{n_\mu}\phi_{n_\mu-1}(x_\mu)\right], \quad \text{(B8)}
$$

together with the orthonormality relation (A3). The total matrix element reads

$$
\langle \alpha;+|\hat{J}_x|\alpha';+\rangle
$$
$$
= \frac{\hbar}{2}(-1)^{n_x+1}\delta_{n_x,n'_x}\delta_{n_y,n'_y}\delta_{n_z,n'_z}
$$
$$
+ \frac{\hbar}{2}\delta_{n_x,n'_x}\left(\frac{b_y}{b_z} - \frac{b_z}{b_y}\right)\left[\sqrt{n'_y + 1}\sqrt{n'_z + 1}\delta_{n_y,n'_y+1}\delta_{n_z,n'_z+1}\right.
$$
$$
\left. + \sqrt{n'_y}\sqrt{n'_z}\delta_{n_y,n'_y-1}\delta_{n_z,n'_z-1}\right]
$$
$$
- \frac{\hbar}{2}\delta_{n_x,n'_x}\left(\frac{b_y}{b_z} + \frac{b_z}{b_y}\right)\left[\sqrt{n'_y + 1}\sqrt{n'_z}\delta_{n_y,n'_y+1}\delta_{n_z,n'_z-1}\right.
$$
$$
\left. + \sqrt{n'_y}\sqrt{n'_z + 1}\delta_{n_y,n'_y-1}\delta_{n_z,n'_z+1}\right]. \quad \text{(B9)}
$$

The following relations can easily be proved:

$$
\langle \alpha;+|\hat{J}_x|\alpha';+\rangle = -\langle \alpha;-|\hat{J}_x|\alpha';-\rangle
$$

and

$$
\langle \alpha;+|\hat{J}_x|\alpha';-\rangle = \langle \alpha;-|\hat{J}_x|\alpha';+\rangle = 0. \quad \text{(B10)}
$$

The final expression for the moment of inertia $\mathcal{I}_x \equiv \mathcal{I}_1$ is

$$
\mathcal{I}_x = 2 \sum_{i,j>0} \frac{(u_i v_j - v_i u_j)^2}{E_i + E_j}\left| \sum_{\alpha\alpha'} f_i^\alpha f_j^{\alpha'}\langle \alpha;+|\hat{J}_x|\alpha';+\rangle \right.
$$
$$
\left. - \sum_{\tilde{\alpha}\tilde{\alpha}'} g_i^{\tilde{\alpha}} g_j^{\tilde{\alpha}'}\langle \tilde{\alpha};+|\hat{J}_x|\tilde{\alpha}';+\rangle \right|^2. \quad \text{(B11)}
$$

We include only the final results for the matrix elements of $\hat{J}_y$ and $\hat{J}_z$:

$$
\begin{aligned}
\langle\alpha;+|\hat{J}_y|\alpha';-\rangle = {} & i\frac{\hbar}{2}(-1)^{n_y}\delta_{n_x,n_x'}\delta_{n_y,n_y'}\delta_{n_z,n_z'} \\
& + i\frac{\hbar}{2}\delta_{n_y,n_y'}(-1)^{n_x+n_y}\left(\frac{b_z}{b_x}-\frac{b_x}{b_z}\right) \\
& \times\left[\sqrt{n_x'+1}\sqrt{n_z'+1}\delta_{n_x,n_x'+1}\delta_{n_z,n_z'+1}\right. \\
& \left.- \sqrt{n_y'}\sqrt{n_z'}\delta_{n_x,n_x'-1}\delta_{n_z,n_z'-1}\right] \\
& + i\frac{\hbar}{2}\delta_{n_y,n_y'}(-1)^{n_x+n_y}\left(\frac{b_z}{b_x}+\frac{b_x}{b_z}\right) \\
& \times\left[\sqrt{n_x'+1}\sqrt{n_z'}\delta_{n_x,n_x'+1}\delta_{n_z,n_z'-1}\right. \\
& \left.- \sqrt{n_x'}\sqrt{n_z'+1}\delta_{n_x,n_x'-1}\delta_{n_z,n_z'+1}\right], \quad\text{(B12)}
\end{aligned}
$$

$$
\langle\alpha;-|\hat{J}_y|\alpha';+\rangle = -\langle\alpha;+|\hat{J}_y|\alpha';-\rangle,
$$

and

$$
\langle\alpha;+|\hat{J}_y|\alpha';+\rangle = \langle\alpha;-|\hat{J}_y|\alpha';-\rangle = 0, \quad\text{(B13)}
$$

$$
\begin{aligned}
\langle\alpha;+|\hat{J}_z|\alpha';-\rangle = {} & \frac{\hbar}{2}(-1)^{n_x+n_y+1}\delta_{n_x,n_x'}\delta_{n_y,n_y'}\delta_{n_z,n_z'} \\
& + \frac{\hbar}{2}\delta_{n_z,n_z'}(-1)^{n_x+n_y+1}\left(\frac{b_x}{b_y}-\frac{b_y}{b_x}\right) \\
& \times\left[\sqrt{n_x'+1}\sqrt{n_y'+1}\delta_{n_x,n_x'+1}\delta_{n_y,n_y'+1}\right. \\
& \left.+ \sqrt{n_x'}\sqrt{n_y'}\delta_{n_x,n_x'-1}\delta_{n_y,n_y'-1}\right] \\
& + \frac{\hbar}{2}\delta_{n_z,n_z'}(-1)^{n_x+n_y+1}\left(\frac{b_x}{b_y}+\frac{b_y}{b_x}\right) \\
& \times\left[\sqrt{n_x'+1}\sqrt{n_y'}\delta_{n_x,n_x'+1}\delta_{n_y,n_y'-1}\right. \\
& \left.+ \sqrt{n_x'}\sqrt{n_y'+1}\delta_{n_x,n_x'-1}\delta_{n_y,n_y'+1}\right], \quad\text{(B14)}
\end{aligned}
$$

$$
\langle\alpha;-|\hat{J}_z|\alpha';+\rangle = \langle\alpha;+|\hat{J}_z|\alpha';-\rangle,
$$

and

$$
\langle\alpha;+|\hat{J}_z|\alpha';+\rangle = \langle\alpha;-|\hat{J}_z|\alpha';-\rangle = 0, \quad\text{(B15)}
$$

The corresponding moments of inertia $\mathcal{I}_y \equiv \mathcal{I}_2$ and $\mathcal{I}_z \equiv \mathcal{I}_3$ read

$$
\begin{aligned}
\mathcal{I}_y = 2\sum_{i,j>0}\frac{(u_iv_j-v_iu_j)^2}{E_i+E_j}\left|\sum_{\alpha\alpha'}f_i^\alpha f_j^{\alpha'}\langle\alpha;+|\hat{J}_y|\alpha';-\rangle\right. \\
\left.- \sum_{\tilde{\alpha}\tilde{\alpha}'}g_i^{\tilde{\alpha}} g_j^{\tilde{\alpha}'}\langle\tilde{\alpha};+|\hat{J}_y|\tilde{\alpha}';-\rangle\right|^2, \quad\text{(B16)}
\end{aligned}
$$

$$
\begin{aligned}
\mathcal{I}_z = 2\sum_{i,j>0}\frac{(u_iv_j-v_iu_j)^2}{E_i+E_j}\left|\sum_{\alpha\alpha'}f_i^\alpha f_j^{\alpha'}\langle\alpha;+|\hat{J}_z|\alpha';-\rangle\right. \\
\left.+ \sum_{\tilde{\alpha}\tilde{\alpha}'}g_i^{\tilde{\alpha}} g_j^{\tilde{\alpha}'}\langle\tilde{\alpha};+|\hat{J}_z|\tilde{\alpha}';-\rangle\right|^2. \quad\text{(B17)}
\end{aligned}
$$

All three moments of inertia vanish at the spherical point $\beta = 0$. In addition, $\mathcal{I}_z$ vanishes for the $\gamma = 0°$ configurations

(prolate deformed, with z as the symmetry axis), whereas $\mathcal{I}_y$ vanishes at $\gamma = 60°$ (oblate deformed, y is the symmetry axis). These conditions are incorporated in the following functional form:

$$
\mathcal{I}_k = 4B_k\beta^2\sin^2(\gamma - 2k\pi/3), \quad\text{with}
$$
$$
(1\equiv x, 2\equiv y, 3\equiv z), \quad\text{(B18)}
$$

from which the inertia parameters B_x, B_y, and B_z follow:

$$
B_k = \frac{\mathcal{I}_k}{4\beta^2\sin^2(\gamma - 2k\pi/3)}. \quad\text{(B19)}
$$

For the limiting cases described above, the following relations are used:

$$
B_x(\beta = 0) = B_y(\beta = 0) = B_z(\beta = 0) = B_{\gamma\gamma}(\beta = 0), \quad\text{(B20)}
$$

$$
B_y(\beta, \gamma = 60°) = B_{\gamma\gamma}(\beta, \gamma = 60°), \quad\text{(B21)}
$$
$$
B_z(\beta, \gamma = 0°) = B_{\gamma\gamma}(\beta, \gamma = 0°). \quad\text{(B22)}
$$

To calculate the mass parameters from Eqs. (45) and (46), one needs the matrix elements of the operators x^2, y^2, and z^2 in the simplex basis. These are combined and inserted into the matrix elements

$$
\begin{aligned}
\langle\psi_i|\hat{Q}_{2\mu}|\psi_j\rangle = {} & \sum_{\alpha\alpha'}f_i^\alpha f_j^{\alpha'}\langle\alpha;+|\hat{Q}_{2\mu}|\alpha';+\rangle \\
& + \sum_{\tilde{\alpha}\tilde{\alpha}'}g_i^{\tilde{\alpha}} g_j^{\tilde{\alpha}'}\langle\tilde{\alpha};+|\hat{Q}_{2\mu}|\tilde{\alpha}';+\rangle, \quad\text{(B23)}
\end{aligned}
$$

which determine the 2×2 matrix $\mathcal{M}_{(n),\mu\nu}$ of Eq. (46). The mass parameters $B_{\mu\nu}(q_0, q_2)$ are then calculated from Eq. (45) and transformed from the quadrupole coordinates q_0, q_2 to the polar Bohr deformation variables β and γ.

APPENDIX C: ROTATIONAL ZERO-POINT ENERGY CORRECTION

The rotational zero-point energy in Eq. (49) is determined by the matrix elements of the quadrupole operators

$$
\hat{Q}_{21} = -2iyz, \quad \hat{Q}_{2-1} = -2xz, \quad\text{and}\quad \hat{Q}_{2-2} = 2ixy. \quad\text{(C1)}
$$

Using the expression

$$
x_\mu\phi_{n_\mu}(x_\mu) = \frac{b_\mu}{\sqrt{2}}\left[\sqrt{n_\mu+1}\phi_{n_\mu+1}(x_\mu) + \sqrt{n_\mu}\phi_{n_\mu-1}(x_\mu)\right], \quad\text{(C2)}
$$

together with the orthogonality relation (A3), the calculation of matrix elements is straightforward. Here we list only the final expressions:

$$
\begin{aligned}
\langle\alpha;+|\hat{Q}_{21}|\alpha';+\rangle = {} & b_yb_z\delta_{n_x,n_x'} \\
& \times\left[-\sqrt{n_y'+1}\delta_{n_y,n_y'+1} + \sqrt{n_y'}\delta_{n_y,n_y'-1}\right] \\
& \times\left[\sqrt{n_z'+1}\delta_{n_z,n_z'+1} + \sqrt{n_z'}\delta_{n_z,n_z'-1}\right], \quad\text{(C3)}
\end{aligned}
$$

$$
\langle\alpha;-|\hat{Q}_{21}|\alpha';-\rangle = -\langle\alpha;+|\hat{Q}_{21}|\alpha';+\rangle, \quad\text{(C4)}
$$

$$\langle\alpha;+|\hat{Q}_{21}|\alpha';-\rangle = \langle\alpha;-|\hat{Q}_{21}|\alpha';+\rangle = 0, \tag{C5}$$

$$\langle\alpha;+|\hat{Q}_{2-1}|\alpha';-\rangle = (-1)^{n'_x+n'_y}b_x b_z \delta_{n_y,n'_y}$$
$$\times\left[\sqrt{n'_x+1}\delta_{n_x,n'_x+1}+\sqrt{n'_x}\delta_{n_x,n'_x-1}\right]$$
$$\times\left[\sqrt{n'_z+1}\delta_{n_z,n'_z+1}+\sqrt{n'_z}\delta_{n_z,n'_z-1}\right] \tag{C6}$$

$$\langle\alpha;-|\hat{Q}_{2-1}|\alpha';+\rangle = -\langle\alpha;+|\hat{Q}_{2-1}|\alpha';-\rangle, \tag{C7}$$

$$\langle\alpha;+|\hat{Q}_{2-1}|\alpha';+\rangle = \langle\alpha;-|\hat{Q}_{2-1}|\alpha';-\rangle = 0, \tag{C8}$$

$$\langle\alpha;+|\hat{Q}_{2-2}|\alpha';-\rangle = (-1)^{n'_x+n'_y+1}b_x b_y \delta_{n_z,n'_z}$$
$$\times\left[\sqrt{n'_x+1}\delta_{n_x,n'_x+1}+\sqrt{n'_x}\delta_{n_x,n'_x-1}\right]$$
$$\times\left[\sqrt{n'_y+1}\delta_{n_y,n'_y+1}-\sqrt{n'_y}\delta_{n_y,n'_y-1}\right], \tag{C9}$$

$$\langle\alpha;-|\hat{Q}_{2-2}|\alpha';-\rangle = -\langle\alpha;+|\hat{Q}_{2-2}|\alpha';+\rangle, \tag{C10}$$

$$\langle\alpha;+|\hat{Q}_{2-2}|\alpha';-\rangle = \langle\alpha;-|\hat{Q}_{2-2}|\alpha';+\rangle = 0. \tag{C11}$$

APPENDIX D: NUMERICAL DETAILS

In Fig. 23, we check the convergence of the RMF+BCS quadrupole constrained calculations as a function of the maximal number of oscillator shells used in the expansion of the Dirac spinors. The binding energy curves for ^{154}Gd are plotted as functions of the axial β deformation. These curves correspond to calculations with 10, 12, 14, and 16 major oscillator shells. For moderate deformations considered in this study ($|\beta| < 0.65$), the RMF results show convergence at $N_F = 14$.

The self-consistent RMF+BCS equations are solved on a mesh over the first sextant of the β-γ plane:

$$\beta \geqslant 0, \quad \Delta\beta = 0.05, \quad 0 \leqslant \gamma \leqslant 60°, \quad \Delta\gamma = 6°, \tag{D1}$$

and the maximum value of the β deformation is $\beta_{\max} = 1.15$.

The choice of the basis wave functions of Eq. (16) introduces a factor $e^{-\mu^2\beta^2}$ into the integral over β in the matrix
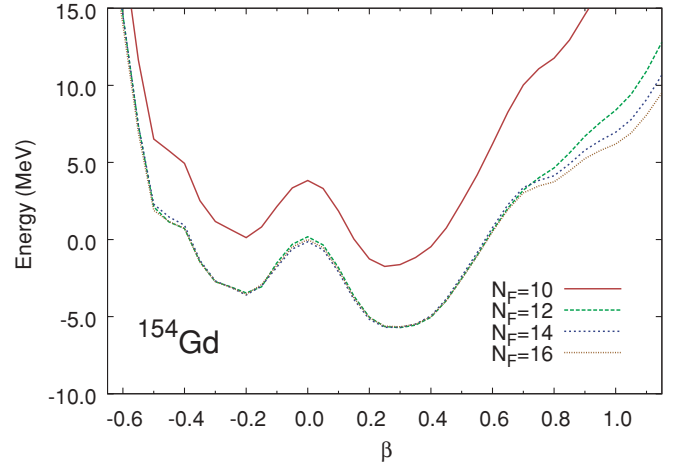

FIG. 23. (Color online) Self-consistent RMF+BCS binding energy curves of ^{154}Gd, as functions of the axial deformation parameter β. Negative values of β correspond to the ($\beta > 0$, $\gamma = 180°$) axis on the β-γ plane. The four energy curves correspond to calculations in the three-dimensional harmonic oscillator basis with 10, 12, 14, and 16 major oscillator shells.

elements of the collective Hamiltonian. With the substitution $y \equiv \mu^2\beta^2$, we obtain the weight function appropriate for Gauss-Laguerre quadrature. The integrals over γ are evaluated by Gauss-Legendre quadrature. The corresponding number of mesh points are $n_\beta = 24$ and $n_\gamma = 24$, respectively. The parameters of the collective Hamiltonian in the Gaussian mesh points are calculated by interpolation from the values calculated on the equidistant mesh in Eq. (D1). To avoid extrapolation, the minimum value of the basis parameter μ is restricted to

$$\frac{\sqrt{y_{n_\beta}}}{\mu} < \beta_{\max}. \tag{D2}$$

We have verified that both the calculated excitation spectra and transition probabilities remain stable for any choice of μ within the interval $8 \leqslant \mu \leqslant 15$. All calculations presented in this work are performed with $\mu = 9$.

[1] M. Bender, P.-H. Heenen, and P.-G. Reinhard, Rev. Mod. Phys. **75**, 121 (2003).

[2] D. Vretenar, A. V. Afanasjev, G. A. Lalazissis, and P. Ring, Phys. Rep. **409**, 101 (2005).

[3] J. Meng, H. Toki, S. G. Zhou, S. Q. Zhang, W. H. Long, and L. S. Geng, Prog. Part. Nucl. Phys. **57**, 470 (2006).

[4] P. Ring and P. Schuck, *The Nuclear Many-Body Problem* (Springer-Verlag, Heidelberg, 1980).

[5] T. Nikšić, D. Vretenar, and P. Ring, Phys. Rev. C **73**, 034308 (2006).

[6] T. Nikšić, D. Vretenar, and P. Ring, Phys. Rev. C **74**, 064309 (2006).

[7] T. Nikšić, D. Vretenar, G. A. Lalazissis, and P. Ring, Phys. Rev. Lett. **99**, 092502 (2007).

[8] M. A. Caprio, Phys. Rev. C **72**, 054323 (2005).

[9] T. R. Rodríguez and J. L. Egido, Phys. Lett. **B663**, 49 (2008).

[10] L. M. Robledo, R. R. Rodríguez-Guzmán, and P. Sarriguren, Phys. Rev. C **78**, 034314 (2008).

[11] M. Bender and P.-H. Heenen, Phys. Rev. C **78**, 024309 (2008).

[12] M. Anguiano, J. L. Egido, and L. M. Robledo, Nucl. Phys. **A696**, 467 (2001).

[13] J. Dobaczewski, M. V. Stoitsov, W. Nazarewicz, and P.-G. Reinhard, Phys. Rev. C **76**, 054315 (2007).

[14] D. Lacroix, T. Duguet, and M. Bender, arXiv:0809.2041; M. Bender, T. Duguet, and D. Lacroix, arXiv:0809.2045; T. Duguet, M. Bender, K. Bennaceur, D. Lacroix, and T. Lesinski, arXiv:0809.2049.

[15] P.-G. Reinhard and K. Goeke, Rep. Prog. Phys. **50**, 1 (1987).

[16] P. Bonche, J. Dobaczewski, H. Flocard, P.-H. Heenen, and J. Meyer, Nucl. Phys. **A510**, 466 (1990).

[17] B. Giraud and B. Grammaticos, Nucl. Phys. **A255**, 141 (1975).

[18] M. Girod and B. Grammaticos, Nucl. Phys. **A330**, 40 (1979).

[19] M. Baranger and M. Veneroni, Ann. Phys. (NY) **114**, 123 (1978).

[20] F. Villars, Nucl. Phys. **A285**, 269 (1977).

[21] K. Goeke and P.-G. Reinhard, Ann. Phys. (NY) **124**, 249 (1980).

[22] R. E. Peierls and J. Yoccoz, Proc. Phys. Soc. London, Sect. A **70**, 381 (1957).

[23] D. J. Thouless and J. G. Valatin, Nucl. Phys. **31**, 211 (1962).

[24] D. R. Inglis, Phys. Rev. **103**, 1786 (1956).

[25] J. Libert, M. Girod, and J.-P. Delaroche, Phys. Rev. C **60**, 054301 (1999).

[26] L. Próchniak, P. Quentin, D. Samsoen, and J. Libert, Nucl. Phys. **A730**, 59 (2004).

[27] L. Próchniak and P. Ring, Int. J. Mod. Phys. E **13**, 217 (2004).

[28] D. A. Varshalovich, A. N. Moskalev, and V. K. Khersonskii, *Quantum Theory of Angular Momentum* (World Scientific, Singapore, 1988).

[29] W. Pauli, in *Handbuch der Physik* (Springer Verlag, Berlin, 1933), Vol. XXIV, p. 120.

[30] K. Kumar and M. Baranger, Nucl. Phys. **A92**, 608 (1967).

[31] S. G. Rohozinski, J. Dobaczewski, B. Nerlo-Pomorska, K. Pomorski, and J. Srebrny, Nucl. Phys. **A292**, 66 (1977).

[32] D. Troltenier, J. Maruhn, W. Greiner, and P. Hess, Z. Phys. A **343**, 25 (1992).

[33] G. G. Dussel and D. R. Bes, Nucl. Phys. **A143**, 623 (1970).

[34] G. Gneuss and W. Greiner, Nucl. Phys. **A171**, 449 (1971).

[35] K. Kumar, Nucl. Phys. **A321**, 189 (1974).

[36] J. Libert and P. Quentin, Phys. Rev. C **25**, 571 (1982).

[37] I. Deloncle, J. Libert, L. Bennour, and P. Quentin, Phys. Lett. **B233**, 16 (2008).

[38] I. Deloncle, Ph.D. thesis, Université de Paris 6, 1989.

[39] L. Próchniak, K. Zajac, K. Pomorski, S. G. Rohoziński, and J. Srebrny, Nucl. Phys. **A648**, 181 (1999).

[40] M. Hammermesh, *Group Theory and Its Applications to Physical Problems* (Addison-Wesley, Reading, Massachusetts, 1962).

[41] L. Próchniak (in preparation).

[42] W. A. Press, B. P. Flannery, S. A. Teukolsky, and W. T. Vetterling, *Numerical Recipes in C: The Art of Scientific Computing* (Cambridge University Press, Cambridge, England, 1988).

[43] T. Bürvenich, D. G. Madland, J. A. Maruhn, and P.-G. Reinhard, Phys. Rev. C **65**, 044308 (2002).

[44] S. T. Belyaev, Nucl. Phys. **24**, 322 (1961).

[45] C. W. Reich and R. G. Helmer, Nucl. Data Sheets **85**, 171 (1988).

[46] N. Zamfir and R. Casten, Phys. Lett. **B260**, 265 (1991).

[47] E. A. McCutchan, D. Bonatsos, N. V. Zamfir, and R. F. Casten, Phys. Rev. C **76**, 024306 (2007).

[48] W. Koepf and P. Ring, Phys. Lett. **B212**, 397 (1988).

[49] J. Dobaczewski and J. Dudek, Comput. Phys. Commun. **102**, 166 (1997).

[50] J. M. Yao, H. Chen, and J. Meng, Phys. Rev. C **74**, 024307 (2006).

[51] J. Peng, J. Meng, P. Ring, and S. Q. Zhang, Phys. Rev. C **78**, 024313 (2008).

[52] Y. K. Gambhir, P. Ring, and A. Thimet, Ann. Phys. (NY) **198**, 132 (1990).